B381.1
I-58

INDO - USSR SEMINAR

ON

SYNCHROTRON RADIATION SOURCE

PREPRINTS OF LECTURES

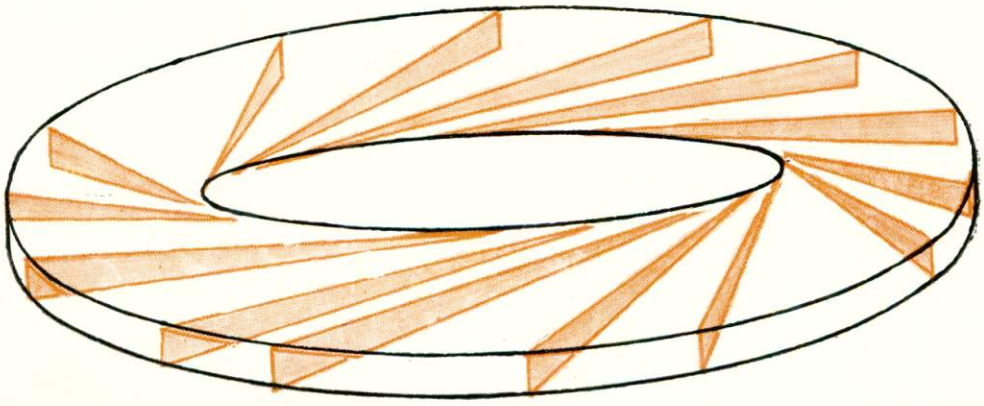

S R
"Moving Searchlight"

Jan. 30 - Feb. 3, 1989

CENTRE FOR ADVANCED TECHNOLOGY

INDORE - 452 012 INDIA

B 381.1
I-58

INDO - USSR SEMINAR

ON

SYNCHROTRON RADIATION SOURCE (SRS)

PHYSICS, TECHNOLOGY & UTILIZATION

Jan. 30 - Feb. 3, 1989

○

Sponsored By :

DEPARTMENT OF SCIENCE & TECHNOLOGY

○

Organised By :

CENTRE FOR ADVANCED TECHNOLOGY

INDORE - 452 012 INDIA

SYNCHROTRON RADIATION SOURCES

G.N.Kulipanov, A.N.Skrinsky
Institute of Nuclear Physics
Siberian Division of the USSR Academy of Sciences
Novosibirsk, USSR

1. INTRODUCTION

The synchrotron radiation (SR) or magnetic bremstrahlung [1-7] during travelling of high-energy charged particles (electrons and positrons) in magnetic field has already been used long and fruitfully in high-energy physics. Synchrotron radiation is a very convenient mean to measure the characteristics of beams in the storage rings and accelerators. Here the sensitivity of the method is the highest achievable - the radiation even a single electron or positron "living" in the storage ring can easily be observed. Especially important is the use of the radiation friction (caused by synchrotron radiation) which enables the compression of beams down to very small sizes and repeated storage of new portions of particles, which is fundamental for obtaining the intense positron beams. Synchrotron radiation leads to appearance of polarization of electeons and positrons, travelling in a storage ring, which permits to obtain the intense polarized beams of electrons and positrons.

But the use of synchrotron radiation for the generation of high-energy beams (as well as for the observation of these luminescent beams) in the field of nuclear physics and physics of elementary particles does not exhaust by far the field of its practical utilization. Still larger importance the use of electron storage rings gains in their use as sources of electromagnetic radiation ranging from the ultraviolet to hard X-ray radiation with an intensity and especially brightness exceeding by many orders of magnitude those from any other sources currently available. The use of synchrotron radiation during the last decade (see, for example, [8-11]) has shown that similarly to that as experiments with electron-positron colliding beams supply at present a substantial fraction of all experimental data in physics of elementary particles, SR experiments already made a substantial contribution into the development of various branches of science (atomic and molecular physics, physics of solid body, catalysis, material science, biophysics). New technologies based on the use of synchrotron radiation are being developed rapidly.

In the paper presented here the potentials of SR sources are characterized as well as the ways and limits for their further improvement are considered. The main fields for the utilization of this class of SR sources are briefly considered.

2. BASIC PROPERTIES OF SYNCHROTRON RADIATION

2.1. Qualitative Characteristics of Synchrotron Radiation of Single Electron

Let us consider the radiation of an ultrarelativistic electron ($\gamma = E/mc^2 \gg 1$, and in the case of interest even $\gamma > 100$ where E - is an electron energy and $mc^2 \simeq 0.5$ MeV - its rest energy), travelling in some magnetic field (of a complex configuration) near a closed trajectory. Just this situation is characteristic of the cyclic accelerators and storage rings of interest to us.

Let, for a sufficiently long portion, an electron trajectory be close to a circle of radius R (Fig. 1). Then the radiation will be concentrated near the orbital plane (the major power is concentrated in an angle of the order $\Psi_{xz} \sim 1/\gamma$). The radiation reaches the point of observation located in this plane along a tangent drawn to the trajectory from this point. The length of trajectory portion providing the main contribution to the radiation power at the selected point of observation will be of the order

$$L_\varphi \simeq \frac{R}{\gamma} = \frac{mc^2}{eH} ,$$

where e is an electron charge, H is the magnetic field at the point of radiation.

The electromagnetic wave radiated by an electron while its single pass will arrive at the point of observation in a form of electric and magnetic field burst having its length of the order

$$\Delta T_c = \frac{L_\varphi}{V} - \frac{L_\varphi}{c} \approx \frac{R}{c\gamma^3} \simeq \frac{mc^2}{\gamma^2 eH} ,$$

where V_c is the velocity of light, V is an electron velocity. Correspondingly, the radiation spectrum will have its maximum at a wave length

$$\lambda_c = \frac{R}{\gamma^3}$$

Note, that the angular divergence of the radiation $\psi \sim 1/\gamma$ at a wave length $\lambda \sim R/\gamma^3$ corresponds to an "effective" transverse size of the source being in the order of magnitude equal to

$$\Delta_{1z} \sim \Delta_{1x} \sim \frac{R}{\gamma^2}$$

The electric and magnetic field at the burst maximum will be

$$E_{max} \approx \frac{4\gamma^4 e}{RD}$$

where D is a distance between the point of observation and the point of radiation. Correspondingly, the energy flux density radiated by a single electron in periodic motion, estimated as a time averaged value of $cE^2/4\pi$ (c is the velocity of light) will be equal to

$$I_1 = \frac{e^4}{m^2c^3} \cdot \frac{H^2\gamma^4}{D^2}$$

The energy flux density I_1 determines the sample illumination at a distance D from the point of radiation.

The total radiation intensity in all directions is

$$P_1 = I_1 S \approx \frac{e^4 H^2}{m^2c^3}\gamma^2,$$

where $S = D^2/\gamma^2$ is the total area of regions illuminated by normal incident synchrotron radiation and located at a distance D from the point of radiation.

Another important characteristic is also the quantity determining the energy loss of an electron per one revolution. If the magnetic field is constant in regions of radiation, the energy loss per one revolution is

$$\Delta W = \frac{4\pi e^4 H^2 \gamma^2}{3m^2c^4} R = \frac{4\pi e^2}{3R}\gamma^4.$$

The total number of quanta of all energies radiated by an electron per one revolution is equal to

$$N_{1\Sigma} \approx \frac{\Delta W \cdot \lambda_c}{\hbar c} \approx \frac{2\pi e^2}{\hbar c} = 2\pi\alpha\gamma,$$

where $\hbar$ is the Plank's constant and α = 1/137 is the fine-structure constant.

For an electron single pass the radiation spectrum at the point of observation will naturally be continuous. For the wave length region of our interest, $\lambda \ll R$, an electron successive passages are uncorrelated in practical cases and the spectrum for this wave-length region for "periodic" motion of irradiating electron remains to be continuous. The radiation intensity in the long wave-length part of the spectrum for $\lambda > \lambda_c$ drops slowly as $(\lambda_c/\lambda)^{1/3}$, and in the short wave-length of the spectrum for $\lambda < \lambda_c$ a rapid exponential drop is observed

$$\sim \sqrt{\lambda_c/\lambda}\, \exp(-\lambda_c/\lambda).$$

One should note, that an angular divergence of radiation with $\lambda_1 > \lambda_c$ is determined by the energy value at which the radiation had its maximum for this wave length $\psi_{\lambda_1} = 1/\gamma_1$, where $\gamma_1 = (R/\lambda_1)^{1/3}$, and therefore, $\psi_\lambda \sim (\lambda/R)^{1/3}$.

The range of angles at which a single electron radiation arrives at the point of observation, after averaging over time can be characterized by introducing an "effective" radial size equal to

$$\Delta_{1x} \sim R\psi_\lambda^2$$

In the vertical direction the situation is more complicated: if the observation point is in the orbital plane, the interval of angles of radiation arrival at the point of observation is zero; with the deviation from the plane it increases linearly and corresponds to a vertical size

$$\Delta_{1z} \sim R\psi_\lambda \frac{\xi}{D},$$

where ξ is the deviation from orbital plane, D is a distance between the observation and radiation points, ψ_λ is an angular divergence of SR at wave length λ. Since the major power is irradiated at a vertical angle $\xi/L = \psi_\lambda$, the "effective" vertical size turns out also to be equal to $R\psi_\lambda^2$.

The electric field intensity vector at the observation point lying in the orbital plane is perpendicular to the tangent drawn from the observation point to an electron trajectory and lies in the orbital plane; the wave magnetic field is perpendicular to the plane, i.e. the radiation in the orbital plane is linearly polarized. If the observation point is outside the orbital plane, the radiation becomes elliptically po-

larized. The rotation direction for radiation field vectors coincides with the electron rotation direction seen from the point of observation. Therefore, on different sides of orbital plane the radiation has its left and right elliptical polarization.

2.2. A Study of an Electron in Periodically Alternating Magnetic Field along the Trajectory

The magnetic field may not be constant along the electron trajectory. Quite an efficient way to enhance the SR intensity is to install the magnetic "snakes"[12-15] producing a sign-alternating periodic magnetic field with a period λ_0 on the trajectory portion of a length $L_{SN} = N\lambda_0$ (N is the number of periodicity elements) (Fig.2).

The field in such a "snake" has its simplest form as follows:

$$H(S) = H_0 \sin \frac{2\pi}{\lambda_0} S.$$

Regardless of the "snake" parameters and electron energy the energy loss for electrons in the "snake" ΔW_{SN} is defined exactly in the same way as that when passing the length L_{SN} in magnetic field H

$$\Delta W_{SN} = \frac{e^4 \gamma^2}{m^2 c^4} \bar{H}_0^2 L_{SN}.$$

The spectral and angular distribution of radiation from the "snake" depends essentially on the ratio between the maximum angle of electron bending in the "snake" magnetic field

$$\alpha_0 = \frac{\lambda_0}{2\pi R} = \frac{\lambda_0 e H_0}{2\pi \gamma mc^2}$$

and radiation angle of electrons from the single magnet $\psi_{xz} \sim 1/\gamma$. Usually, this ratio is characterized by the so-called undulator parameter

$$K = \alpha_0 \gamma = \frac{\lambda_0 e H_0}{2\pi mc^2},$$

which just determines the "snake" operational run.

2.2.1. Undulator Mode

At low fields $K \ll 1$ the transverse motion of electrons in the "snake" in non-relativistic and the value of an elec-

tron longitudinal velocity modulation during its motion in the "snake" can be neglected. An electromagnetic wave, irradiated by an electron for its single pass of the "snake", arrives at the point of observation located along the "snake" axis in the form of bursts of electric (magnetic) field spaced in time by

$$T_1 = \frac{\lambda_0}{V_{11}} - \frac{\lambda_0}{c}$$

(where V_{11} is an electron velocity along the "snake" axis). Due to the curved trajectory in the "snake" the electron longitudinal velocity along the axis S will be equal to

$$V_{11} = V\left(1 - \frac{\alpha_0^2}{4}\right)$$

, therefore

$$T_1 = \frac{\lambda_0}{V\left(1 - \frac{\alpha_0^2}{4}\right)} - \frac{\lambda_0}{c} = \frac{\lambda_0}{2\gamma^2 c}\left(1 + \frac{\alpha_0^2\gamma^2}{2}\right).$$

Correspondingly, at the point of observation on the S -axis the radiation is detected with a wave length

$$\lambda_{und} = T_1 c = \frac{\lambda_0}{2\gamma^2}\left(1 + \frac{\alpha_0^2\gamma^2}{2}\right) = \frac{\lambda_0}{2\gamma^2}\left(1 + \frac{K^2}{2}\right).$$

The source of radiation is moving with a velocity $V_{11}\cos\Theta$ to the point of observation located at an angle Θ with respect to the "snake" axis. At this point the radiation is detected with a wave length

$$\lambda_{und} = \frac{\lambda_0}{2\gamma^2}\left(1 + \frac{K^2}{2} + \gamma^2\Theta^2\right).$$

In the undulator case, the radiation monochromaticity is determined by the length of wave train and correspondingly by the number of irradiators

$$\frac{\Delta\lambda}{\lambda} \sim \frac{1}{N}.$$

An angular divergence for undulator radiation at zeroth angle is

$$\Delta\Psi_{oz} \sim \Delta\Psi_{ox} \sim \sqrt{\lambda / L_{und}} \sim \frac{\sqrt{1 + K^2/2}}{\gamma\sqrt{N}}.$$

This angular divergence of undulator radiation corresponds to the "effective" transverse size of the source being equal to

$$\Delta_{iz} \sim \Delta_{ix} \sim \sqrt{\lambda L_{und}}.$$

The total number of quanta irradiated by an electron during its pass through an undulator is

$$N_{1und} = \frac{\Delta W_{SN}\,\lambda_{und}}{\hbar c} \sim \frac{1}{137} N (\alpha_0 \gamma)^2 .$$

An axial radiation of the undulator with transverse magnetic field is linearly polarized, and axial radiation for the undulator with helical magnetic field is circularly polarized.

2.2.2. Harmonics Generation Mode for Undulator Radiation ($K \gtrsim 1$)

With the increase in the "snake" magnetic field the value K grows, an electron transverse motion becomes relativistic, the electron longitudinal velocity modulation along the "snake" axis becomes substantial. In this case the undulator radiation harmonics appear in the spectrum of radiation ($i = 1,2,3\ldots$)

$$\lambda_i = \frac{\lambda_0}{2i\gamma^2}\left(1 + \frac{K^2}{2} + \gamma^2\theta^2\right).$$

The parameter K determines the relation of two time value characteristics for radiation from the "snake" at a large field.

The first time value is the burst duration of the electric (magnetic) field from a single magnet, which is detected by an observer

$$\Delta T_{CH} \sim \frac{mc}{\gamma^2 e H_0} .$$

The second time value is an interval between bursts of electric (magnetic) field, irradiated from neighbouring magnets

$$\Delta T_{und} = \frac{\lambda_0}{2\gamma^2 c}\left(1 + \frac{K^2}{2} + \gamma^2\theta\right) .$$

The ratio of these two values

$$\frac{\Delta T_{und}}{\Delta T_{CH}} \sim K\left(1 + \frac{K^2}{2}\right)$$

just determines the number of harmonics providing a substantial contribution into the total power of radiation from the "snake" (see Fig. 7).

2.2.3. Synchrotron Mode ($K>>1$)

Within the range of large magnetic fields ($K>>1$) the radiation characteristics from the given part of trajectory are determined by the trajectory local curvature. The SR flux characteristics at the point of observation are obtained by summing fluxes from different parts of the trajectory.

The use of "snakes" at $K>>1$ can be useful for the solution of various problems related to SR generation:

- obtaining the harder X-ray SR beams at a given electron energy in a storage ring due to the use in "snakes" of superconducting magnets with a field of up to 120 kθe;
- an increase in the power and brightness of X-ray SR beams when using the multipole "snakes" ($N = 50 - 200$).

2.3. Coherent Synchrotron Radiation

If in a storage ring there are N_e travelling electrons, then in the standard case of currently available storage rings the relative positions of electrons one can consider correlated only with an accuracy to the length of bunches of electrons (on the order of 1 cm or larger). In this case, the radiation in the short wave-length region interesting to us is incoherent and energy fluxes of individual electrons I_1 are just summed, i.e. $I_N = N_e I_1$. Though, if electrons are bunched even on a short section of an orbit into bunches of a length 10-0.1 micron, then in a visible and ultraviolet part of the spectrum the radiation will be coherent and energy flux from N_e electrons $I_N = N_e^2 I_1$ will be by a factor N_e larger than that for usual synchrotron radiation. Taking into account that N_e is very large (of the order of 10^8-10^{11}) the problem becomes quite interesting. The coherent SR was extensively explored in the 1950-s. Though, the invention of laser on the one hand, and poor parameters of electron beams atthat time, on the other hand, stopped the development of this work. The generation of coherent radiation in the infra-red region with the help of the "free-electron laser" (undulator surrounded by optic resonator) installed on the beam from linear accelerator /16/ stimulated the attempts to consider the possibilities for

bunching electrons in storage rings into the bunches of 10 - - 0.1 long. The idea of "Optic Klystron" [17] enabled one to obtain the coherent radiation at currently available storage rings for the wave lengths ranging from infra-red to ultraviolet[18].

2.4. Quantitative Data on Synchrotron Radiation Properties

In this section in a form convenient for practical calculation we shall present basic formulae characterizing the properties of synchrotron radiation of electrons from bending magnet of the "snake" and undulator. In these formulae we used the following main parameters: E (GeV) - energy of electrons; $I(a) = 1.6 \times 10^{-19} N_e f_0$ s^{-1} - the storage ring current (N_e is the number of particles, f_0 is the revolution frequency); $H(\kappa Gs)$ is the magnetic field at the radiation point; $R(M) = \frac{100}{3} \frac{E\,GeV}{H\,\kappa Gs}$ is the radius of curvature of electron trajectory, $D(M)$ is a distance between the radiation and observation points.

2.4.1. Radiation from Bending Magnets

The characteristic wave length of synchrotron radiation

$$\lambda_{C\mathring{A}} = \frac{5,59\,R_M}{E^3_{GeV}} = \frac{186,4}{H_{\kappa Gs} E^2_{GeV}}$$

The characteristic energy of SR quanta

$$E_{c\,keV} = 2,21 \frac{E^3\,GeV}{R_M} = 6,65 \cdot 10^{-2} E^2_{GeV} H_{\kappa Gs}.$$

SR beam power is a power of synchrotron radiation summed over all wave lengths, integrated over vertical angle, per milliradian of radial angle

$$P_{.w/mrad} = \frac{14,1\,E^4_{GeV} I_a}{R_M} = 0,43\,H_{\kappa Gs} E^3_{GeV} I_a .$$

Flux of quanta is the total number of quanta of all energies radiated by electrons per milliradian of radial angle:

$$\dot{N}_\Sigma \text{ photons/s mrad} = 1.3\ 10^{17} E_{GeV} I_a .$$

Illumination is the SR beam power summed over all wave lengths per 1 mm^2 area in the orbital plane located at a distance D from the point of radiation

$$I_{\Sigma\ W/MM^2} = \frac{18 E^5_{GeV} I_A}{R_M D^2_M} = \frac{0{,}54\ E^4_{GeV} H_{KGS} I_A}{D^2_M}.$$

Spectral power (spectral flux of quanta) is a power (flux of quanta) at a given wave length λ within the relative wave-length interval $\Delta\lambda/\lambda$

$$P(\lambda)_{W/mrad} = 48 \frac{E^2_{GeV} I_A \eta(\lambda/\lambda_c)}{\lambda_A} \frac{\Delta\lambda}{\lambda}$$

$$\dot{N}(\lambda)_{photons/s\ mrad} = 2.46 \cdot 10^{16} E^2_{GeV} I_A \eta(\lambda/\lambda_c) \cdot \frac{\Delta\lambda}{\lambda},$$

where $\eta(\lambda/\lambda_c)$ is a universal spectral function (Fig. 3). For $\lambda/\lambda_c \gg 1$ and $\lambda/\lambda_c \ll 1$ one can use simple formulae:

$$\dot{N}(\lambda)\ \text{photons/s mrad} = 9.35 \cdot 10^{16} I_A \left(\frac{R_M}{\lambda_A}\right)^{1/3} \frac{\Delta\lambda}{\lambda} \quad \left(\frac{\lambda}{\lambda_c} \gg 1\right)$$

$$\dot{N}(\lambda)\ \text{photons/s mrad} = 3.08 \cdot 10^{16} I_A E_{GeV} \left(\frac{\lambda_c}{\lambda}\right)^{1/2} e^{-\lambda_c/\lambda} \frac{\Delta\lambda}{\lambda} \quad \left(\frac{\lambda}{\lambda_c} \ll 1\right)$$

Angular distribution. An angular distribution width of radiation with $\lambda \sim \lambda_c$

$$\Psi_{\lambda c}\,(\text{mrad}) = \sqrt{2\pi}\,\sigma_r'$$

σ_r' is an effective root-mean-square angle of radiation divergence in vertical plane

$$\sigma_r' = 0.32 \frac{\nu(\lambda/\lambda_c)}{E_{GeV}}$$

where $\nu(\lambda/\lambda_c)$ is a universal angular function (Fig. 4). For

$$\lambda = \lambda_c \quad \sigma_r'\,mrad = 0.32/E_{GeV}$$

$$\lambda \gg \lambda_c \quad \sigma_r'\,mrad = 0.36\,(\lambda/\lambda_c)^{1/3} I/E_{GeV}$$

$$\lambda \ll \lambda_c \quad \sigma_r'\,mrad = 0.21\,(\lambda/\lambda_c)^{1/2} I/E_{GeV}.$$

The form of radiation intensity dependence of an angle value is also a function of parameter λ/λ_c; three characteristic dependences for λ/λ_c = (0.1; 1; 10) are given in Fig.5.

Spectral illumination is a power (photon flux) at a given wave length λ in a wave-length interval $\Delta\lambda/\lambda$ for a 1 mm^2

area located in the orbital plane at a distance D from the point of radiation

$$I_{\lambda\ w/mm^2} = 26\,\frac{E^2_{GeV}\,I_A}{D^2_M\,\lambda_A}\,h\left(\lambda/\lambda_c\right)\cdot\frac{\Delta\lambda}{\lambda}$$

$$I_{\lambda\ photons/mm^2 s} = 1.33\cdot 10^{16}\,\frac{E^2_{GeV}\,I_A}{D^2_M}\,h\left(\lambda/\lambda_c\right)\cdot\frac{\Delta\lambda}{\lambda},$$

where $h(\lambda/\lambda_c)$ is a function which takes into account the spectral characteristics of radiation intensity and angular distribution (see Fig. 3).

Polarization. Degrees of linear and circular polarization defined in the usual way

$$\rho = \frac{I_{\parallel} - I_{\perp}}{I_{\parallel} + I_{\perp}}, \qquad q = \frac{2\left(I_{\parallel}\cdot I_{\perp}\right)^{1/2}}{I_{\parallel} + I_{\perp}},$$

(where $I_{\parallel}$ and $I_{\perp}$ the intensities of radiation polarized parallel and perpendicular to the orbital plane, having a phase shift of $\pm\frac{\pi}{2}$, are functions of the wave length and vertical angle. Fig; 5 shows angular dependences of $I_{\parallel}$, $I_{\perp}$, ρ and q for three values of λ/λ_c = (0.1; 1; 10). In the orbital plane ($\psi = 0$) the radiation is completely polarized linearly ($\rho = 1$, $q = 0$); in the case where $\psi > \psi_1$ the radiation is polarized elliptically ($\rho \to 0, q \to 1$). For the given wave length the radiation linear polarization degree averaged over vertical angle

$$\bar{\rho}(\lambda) = \frac{\int_0^{\infty}\rho(\lambda,\psi)\,N(\lambda,\psi)\,d\psi}{\int_0^{\infty}N(\lambda,\psi)\,d\psi}$$

is a universal function of λ/λ_c plotted in Fig. 6. In the case when $\lambda >> \lambda_c$, we have $\bar{\rho}$ = 50% and in the other limit case where $\lambda << \lambda_c$, we have $\bar{\rho}$ = 100%. If the radiation intensity is integrated over all wave lengths and vertical angles, the intensity of radiation with polarization parallel to the orbital plane turns out to be 7 times larger than that with perpendicular polarization. Therefore, the degree of linear polarization averaged over all wave lengths and angles is 75 %.

2.4.2. Undulator Radiation ($K \gtrsim 1$)

Undulator parameter

$$K = \alpha_0\gamma = 9.34\cdot 10^{-2}\,H_{xGs}\,\lambda_{o\,sm}$$

$$\alpha_{o\ mrad} = 4.77\ 10^{-2}\ \frac{H_{kGs}\lambda_{o\ sm}}{E_{GeV}} -$$

bending angle of an electron in the field of undulator $\gamma =$ $= 1957$, E_{GeV} is relativistic factor, H_o is an amplitude of undulator field, λ_o is a period of variation for the undulator magnetic field.

Radiation wave length along the undulator axis

$$\lambda_A^o = \frac{13,06 \cdot \lambda_{o\ sm}}{i \cdot E_{GeV}^2}\left(1 + \frac{K^2}{2}\right)$$

i is the number of harmonics.

Corresponding energy of photons is

$$\mathcal{E}_{KeV} = 0,950\ \frac{E_{GeV}^2 \cdot i}{1 + K^2/2}\ .$$

Radiation monochromaticity of i-th harmonics from the undulator is

$$\frac{\Delta\lambda}{\lambda} \sim \frac{\Delta\mathcal{E}}{\mathcal{E}} = \frac{1}{iN}$$

N is the number of undulator periods, $L_o = N\lambda_o$ is the undulator total length.

Beam power of undulator radiation

$$P_W = 6,33\ E_{GeV}^2 H_o^2\ L_{om}\ I_A = 36.5\ E_{GeV}^2 N K^2 I_A / \lambda_{o\ sm}$$

Spectral power (spectral flux of quanta) of undulator radiation for i-th harmonic along the undulator axis within the interval $\frac{\Delta\lambda}{\lambda}$.

$$P_{\lambda i\ \frac{kW}{\Delta\lambda/\lambda}} = \frac{0.284}{\lambda_i \text{Å}}\ N\ I_A\ q_i(K) \cdot \frac{\Delta\lambda}{\lambda}$$

$$N_{\lambda i\ \frac{photons}{s\ \Delta\lambda/\lambda}} = 1.43 \cdot 10^{17} \cdot N \cdot I_A\ q_i(K)\ \frac{\Delta\lambda}{\lambda}\ ,$$

where $q_i(K)$ is a spectral function for different harmonics (see Fig. 7).

Angular distribution of i-th harmonic radiated along the undulator axis

$$\sigma'_{r\ mrad} = \sqrt{\frac{\lambda_i}{L_o}} = \frac{0.51}{E_{GeV}}\sqrt{\frac{1 + K^2/2}{2 \cdot N \cdot i}}$$

$L_o = N\lambda_o$ is an undulator total length.

Spectral illumination is a flux of quanta on i-th harmonic within the interval $\Delta\lambda/\lambda$ for a 1 mm^2 area located on the undulator axis at a distance D from the point of radiation

$$I_\lambda \frac{photons}{mm^2 \frac{\Delta\lambda}{\lambda}} = 1{,}74 \cdot 10^{17} \frac{N^2 \cdot E^2_{GeV} I_A}{D^2_M} f_i(K) \frac{\Delta\lambda}{\lambda},$$

where $f_i(K)$ is a spectral angular function for different harmonics (see Fig. 7).

2.4.3. Radiation from "Snake" ($K \gg 1$)

Due to variation of magnetic field along the "snake" axis ($H(s) = H_o \cos \frac{2\pi s}{\lambda_o}$) the characteristic wave length of SR from the "snake" depends on angle Θ (Θ is an observation angle with respect to the "snake")

$$\lambda_c(\Theta) = \lambda_c(0) \frac{1}{\cos\beta}$$

$$\varepsilon_c(\Theta) = \varepsilon_c(0) \cos\beta$$

where $\lambda_c(0)_{\text{Å}} = \frac{186{,}4}{H_{oKGs} E^2_{GeV}}$, $\varepsilon_{cKeV}(0) = 6.65 \cdot 10^{-2} E^2_{GeV} H_{oKGs}$,

and $\sin\beta = \Theta/\alpha_o$, $\left(\alpha_o = 4{,}77 \cdot 10^2 \frac{H_{KGs}\lambda_{o\,sm}}{E_{GeV}}\right.$

is an electron bending angle in the "snake" magnetic field.)

In order to find out the SR beam characteristics along the "snake" axis (power, illumination, spectral power and spectral illumination) in the corresponding formulae for characteristics of SR beam from bending magnets the right-hand sides should be multiplied by a factor $2N$ (N is the number of "snake" periods) and H should be replaced by the value of the "snake" magnetic field amplitude $H = H_o$. And for finding out the SR beam characteristics at an angle Θ with respect to the "snake" axis, one should replace H by the following value

$$H = H_o \cos\beta$$

(where $\sin\beta = \Theta/\alpha_o$).

3. EFFECT OF ELECTRON BEAM PARAMETERS ON THE CHARACTERISTICS OF SYNCHROTRON RADIATION FLUXES

For the majority of cases the main user characteristics of SR is the source brightness (B_λ) in the given part of a spectrum /8/ being equal to the number of photons radiated per unit time from the source unit area into a unit solid angle

$$B_\lambda = \frac{\dot{N}(\lambda)}{S \cdot \Omega} ,$$

where $\dot{N}(\lambda)$ is a spectral flux of photons from radiation source, S is an area of radiation source, Ω is a solid angle of a source.

The brightness depends essentially on the size ($\sigma_{x,z}$) and on electron beam angular spread ($\theta_{x,z}$). Since

$$\sigma_{x,z} \cdot \theta_{x,z} = \varepsilon_{x,z} ,$$

where $\varepsilon_{x,z}$ is an electron beam phase volume, the most important condition for the brightness enhancement is the minimization of a phase volume of an electron beam which in an electron storage ring is determined by equilibrium between the quantum excitation and radiation damping.

In addition, for obtaining the higher brightness of a source the magnetic structure of an electron storage ring should incorporate the straight sections sufficiently long for installing there the "snakes" and undulators. On their azimuths an electron beam should have its transverse dimensions and angular spread optimal for installing the "snakes" and undulators. In the centers of straight sections

$$\sigma_{x,z} = \sqrt{\varepsilon_{x,z} \cdot \beta_{x,z}} \quad ; \quad \theta_{x,z} = \sqrt{\frac{\varepsilon_{x,z}}{\beta_{x,z}}} ,$$

where $\beta_{x,z}$ is an effective focal distance of magnetic system.

Taking into account a large length of the source, for the effective transverse dimensions of beams from "snakes" and undulators we have

$$\Delta_{x,z} = \sqrt{\sigma_{x,z}^2 + (\lambda L + \theta_{x,z}^2 L^2)}$$

An angular divergence for SR beams from "snakes" and undulators is determined by the radiation angular divergence and an angular spread of electrons in a beam

$$\Delta_{x'}, \Delta_{z'} = \sqrt{\psi_\lambda^2 + \theta_{x,z}^2} .$$

Therefore, for optimizing the strong field "snake" parameters in favour to maximum brightness one should compress the size of an electron beam at the point of the "snake" location by reducing $\beta_{x,z}$ at the point of radiation as it is done at interaction points for enhancing the luminosity of colliding beams (straights with a low β -function); it is reasonable to reduce the size until an angular spread in electron beam exceeds an angular divergence of synchrotron radiation. Taking this into account at the place of "snake" location we should have

$$\beta_{x,z} \gtrsim L_{SN}$$

The efficiency of "snakes" in undulator regime strongly depends on an angular spread of electeons in a beam. For obtaining the beams of undulator radiation with $\Delta\lambda/\lambda \sim \frac{1}{N}$ and brightness $B_{und} \sim N^2$ (N is the number of undulator periodicity elements) one has to provide along the entire undulator length the radiation interference condition from electrons having an angular spread $\theta_{x,z}$.

$$L_{und} \cdot \theta_{x,z}^2 < \frac{\lambda_{und}}{\pi}$$

This leads to the following requirement:

$$\varepsilon_{x,z} < \frac{\lambda_{und}}{\pi} \cdot \frac{L_{und}}{\beta_{x,z}}$$

Correspondingly, the sections designed for installing "snakes" should have large $\beta_{x,z}$ function. It is interesting to note, that an ultimate brightness of a source is achieved in the case $\varepsilon_{x,z} < \lambda$. In this case, the whole flux of quanta from undulator has a spatial coherence.

The requirement to minimize the phase volume $\varepsilon_{x,z}$ and to obtain optimum characteristics of magnetic focusing system of storage ring ($\beta_{x,z}$) at the same time determines the storage ring structure. It is characteristic that regardless of the structure an electron beam phase volume is determined by an energy and one geometric characteristic - bending angle φ_m in dipole magnets superperiods /20/

$$\varepsilon_{x\,min} \sim E^2 \varphi_m^3$$

In the storage rings - dedicated SR sources - additionally to the solution of problems of brightness enhancement one should envisage the possibilities of a more complete use of other SR features.

For example, SR beam output from the region where its vertical size is expanded and an angular spread of electrons in a beam is reduced to the value substantially less than the SR divergence (section with large β-function) will enable one by using geometric diaphragming of SR beam to separate the radiation with a high degree of linear and circular polarization not only in the vacuum ultraviolet region, but also in the region of hard X-ray radiation.

In order to obtain the time modulation for SR intensity in a wide range of times ($10^{-11} \div 1$ s) in the specialized source of SR one has to envisage:

- a special system of synchronization in order to provide the storage ring operation either in the single-bunch mode or in the mode of n-bunches, following in a time interval $\Delta t = T/n$ (T is time of particle revolution in a storage ring);
- RF system allowing the bunch lengths of 0.1-1 cm.

For the development of electron storage rings - specialized technological sources of synchrotron radiation the properties as the simplicity, reliability and low cost are becoming very important. Such storage rings actually can be much simpler than those currently existing sources. Although the sources of X-ray range (wave lengths of the order of 1 A and shorter) will remain large installations and it is reasonable to design them for large scientific centres. But the source with its upper limit of irradiated spectrum of tens Å is quite an acceptable source for some institutes, large laboratories and industrial plants.

4. ORGANIZATION OF WORK AND SET UP OF EXPERIMENTS WITH SYNCHROTRON RADIATION

Modern studies with the use of synchrotron radiation are carried out in national centers of synchrotron radiation based either on electron-positron storage rings designed for experiments in physics of elementary particles, or on specialized storage rings - SR sources which, as a rule, are equipped with special "snakes" and undulators. There are five such centers in the USA (Stanford, Madison, Washington, Cornell, Brookhaven).

There are six national centers in Europe (Hamburg - FRG, BESSY - West Berlin, ORSAY - France, DARESBURY - Great Britain, FRASCATY - Italy, LUND - Sweden), four centers function in Japan (Tokyo, ETL, Okasaki, Tsukuba).

Large SR centers are under construction in Berkeley and Argonne (USA), Dortmund (FRG), Triest (Italy) and large SR center is under development in Apuhi (Japan) for the use of SR in microelectronics.

The main research with synchrotron radiation in the Soviet Union are carried out at the Institute of Nuclear Physics of Siberian Division of the USSR Academy of Sciences on the base of which the Siberian Center of Synchrotron Radiation has been created and at the Institute of Atomic Energy named after I.V.Kurchatov where Moscow Center of Syhchrotron Radiation is created on the base of electron storage ring "Siberia--1". The organization of work on the base of SR Center has substantial advantages due to uniting the efforts of many institutions for the development of the required equipment, exchange of experimental experience between various groups.

At the Institute of Nuclear Physics of Siberian Division of the USSR Academy of Sciences there are three storage rings - the SR sources within the range of vacuum ultraviolet and soft X-ray radiation (VEPP-2M) and in the range of hard X-ray radiation (VEPP-3, VEPP-4). Experiments with synchrotron radiation are carried out by a great number of experimental groups from various institutions of Novosibirsk, Moscow, Leningrad, Gorky, Sverdlovsk, Tartu and other cities of our country and also from abroad (DDR, Hungary, CSSR, India, France). The Institute of Nuclear Physics is involved in setting up various experiments with synchrotron radiation relating to the SR source, the use of modern physical equipment, automation and computer control of experiments, development and manufacture of various detectors, spectrometers etc.

The experimental installations are supplied with synchrotron radiation from the storage ring through the special channels. For the work with vacuum ultraviolet or soft X-ray radiation these channels connect directly the storage ring vacuum chamber with vacuum chambers of various experimental installations. X-ray radiation can be put out along the channel directly into atmosphere thro[illegible] window with berilium

БИБЛИОТЕКА
Института ядерной
физики СО АН СССР
ИНВ. № 4/1D-400/2001

foil.

One of the main elements of experimental stations is a monochromator. The crystals, multilayer structures, Frenel zone plates, diffraction gratings are used as monochromators.

Behind the monochromator the radiation reaches the subject of a study: crystal, protein, muscle, catalyst, rock, polymer, metal, etc. The subject studied is usually located in a special chamber which allows to maintain necessary conditions during experimental run (temperature, pressure, special medium, magnetic or electric field, etc.).

The study of interaction between the radiation and the subject supplies various information. There are many methods allowing to define the spatial location of atoms and molecules in a substance, to detect minor admixtures of other elements, to measure characteristics of electron levels and their excited states in atoms, to find out the defects in crystallic structure, to measure the distribution of electrons density, etc. The methods are based on the study of spectra of absorption, reflection, fluorescence, photoelectron emission. For crystal structures very informative is the measurement of angular distribution of the diffracted or diffusively scattered quanta.

Therefore, the next important part of experimental station is a detector which enables the detection both of the primary flux of quanta interacted with the subject under study and the secondary radiation (fluorescence, emission) excited by incident primary flux of quanta. Depending on the experimental requirements the detector should measure with a high accuracy fluxes of quanta, their energy, spatial distribution, and have a high time resolution. The use of synchrotron radiation required the development of new equipment adequate to the source. For example, X-ray photofilm was successfully used in the work with X-ray tubes for the detection of diffraction pictures, in medical diagnostics. An efficient use of synchrotron radiation in these and similar experiments became possible with the development of fast-action detectors, various systems of visualization allowing the fast detection storage and reproduction of the data obtained.

As a rule, each experimental station has an electronic set which in combination with computer is used for the automation of experiments.

For the study with synchrotron radiation performed at INP[11] the following experimental stations have been used.

X-ray lithography. There are five groups involved in the studies on X-ray lithography. The used equipment comprises two X-ray lithography stations, device for matching in vertical plane, lithography technological section, and scanning electron microscope. Their experimental capabilities are the following: testing of resists, patterns, optimization of X-ray lithography technique, testing of the matching and thermal stabilization systems, improving of the technology of monolayer and multilayer X-ray lithography.

Ultra-soft X-ray spectroscopy. There are 6 experimental groups taking part in the work. The used equipment is: a monochromator RSM-500 covering the wave-length range λ = 300÷35 Å with diffraction spherical gratings of 2 and 6 m radius (600 and 120 lines per mm), full external reflection mirror for the suppression of highest-order reflections, a set of sample chambers and detectors. Examples of research work can be: the study of absorption and excitation spectra of the luminescence of ion crystals, the study of the fine structure of absorption edges of complex compounds by the yield of Auger-electrons as well as the measurement of reflection coefficients for X-ray multilayer mirrors.

Time-resolved VUV-spectroscopy. The work is performed by 4 groups. The experimental equipment used is: a monochromator based on the filters with $\Delta\lambda \sim$ 30 Å for luminescence excitation monochromator MDP-2 for measuring the luminescence spectra and a dissector-based detector operated in the stroboscopic mode with a time resolution above 100 ps. The experimental possibilities of the station are: the study of fast fluorescence with a time resolution in a subnanosecond range, the detection of instantaneous luminescent spectra.

VUV-spectroscopy. Seven groups are involved in this work. The equipment used is: a Wardsworth-scheme monochromator, which covers the 300÷5000 Å wave-length range, with a spherical diffraction grating of 2 mm radius (600 and 1200 lines per mm), a set of sample chambers and detectors. The examples of studies are: the study of zone structure of semiconductors and the semiconductor-dielectric structures, finding out the valence electron densities in semiconductors, measurement of

optical constants of semiconductors and compounds, absolute calibration of photomultipliers and photoelements.

X-ray microscopy using beams of undulator radiation. The equipment used is: the lithographic station, electron scanning microscope. The brightness and the spatial coherent region of helical undulator radiation have been measured. The possibilities of a contact X-ray and holographic microscopy are studied.

Photoelectron spectroscopy. The equipment used is: a grazing-incidence grating monochromator covering the 20-2000 Å range, a photoelectron spectrometer. In the studies two experimental groups are involved.

Trace-element analysis. The work at the experimental station is performed by 15 groups. The equipment used is: a single-crystal focusing monochromator with $\Delta\lambda/\lambda \sim 1\%$ (it covers the 5-100 keV energy range), a sample chamber with a scanner, a semiconductor Si(Li) and Ge detectors with an energy resolution of 200 eV and 170 eV, respectively, and fast spectrometric equipment. This experimental station permits to perform an express multi-element analysis of substances with concentrations of 10^{-6} g/g and geo-chemical analysis of ores, moon ground, meteorites with a sensitivity of 10^{-8} g/g. The examples of studies: a search for new ore deposits, technological control of products of metallurgical plants, analysis of the ocean deposits, microelement analysis for biology and medicine.

X-ray topography and diffractometry. The experimental station is used by 9 groups. It is equipped with a goniometer for the "white" X-ray topography, a monochromator for X-ray topography using the monochromatized SR, a diffractometer, a set of sample chambers and detectors. The experimental possibilities are:the visualization of the defects in crystals within the 0.1-2 Å range with a resolution of about 1 m on photoemulsions and 20-50 μm on TV-tubes, the recording of X-ray topographic pictures by video tape-recorders, obtaining the sectionalized topograms of perfect crystals, staheometry of heavy elements in solid solutions by an integrated reflection coefficient. The samples of research work performed at this station: the study of KPT crystals, phase transitions in ferroelectrics, production sorting of natural minerals, express-topography of semiconductor crystals for electronic in-

dustry, a study of the defect structure of complex crystals, the phase transitions in them, a study of the contrast mechanism for X-ray images of the defects in garnets.

X-ray diffraction cinema. 19 experimental groups are involved in this work. The experimental station is equipped with the single-crystal and two-crystal monochromators covering the 3-40 keV range, the one-dimensional and two-dimensional X-ray detectors, a set of sample chambers allowing the experiments in a wide range of temperatures, pressures and mechanical tensions. The experimental possibilities are: a study of the kinetics of the structural changes in the objects with a time resolution exceeding 1 ms. The examples of research work: the study of phase transitions at superhigh pressures, the study of the destruction dynamics in metals, three-dimensional strain measurement, the study of chemical reaction kinetics for SES-processes, structural transformations in solid-state materials during chemical reactions, melting and crystallization processes.

EXAFS-spectroscopy. The experimental station is exploited by 13 groups. The station is equipped with a double-crystal monochromator with $\Delta\lambda/\lambda \sim 2 \cdot 10^{-4}$, ionization chambers for monitoring and a set of sample chambers. The experimental possibilities are the following: the absorption EXAFS-spectroscopy, fluorescent EXAFS-spectroscopy. The examples of research are: the study of the structure of amorphous semiconductors and metallic glasses, the study of structural homology of Ca-bounding proteins, coordiantion of compounds in solutions, the study of metal clusters (layed on oxide sub-layers), various catalysts.

Small-angle diffractometry. There are 3 groups at the experimental station. The station is equipped with a single-crystal monochromator, small-angle chamber, X-ray detector, and a set of sample chambers. The experimental possibilities are: the studies of the structural changes in objects with the structures up to 1000 A with resolution higher than 1 ms, small-angle diffusion scattering. The example of investigations: a study of dynamics of structural changes in muscle with the stimulation by paired electric pulses.

Medicine and X-ray microscopy. Three groups are involved in this work. The experimental station is equipped with a fast-tuning double-crystal monochromator covering the 3-0.2 Å

wave-length range, ionization chambers, scintillation detector and under the development are a new super-fast one-coordinate detector and scanning mechanism. The experimental possibilities are: scanning differential X-ray microscopy of biological objects, examination of the pathology of the human circulatory system. The example of investigation: scanning differential X-ray microscopy of lymphatic nodes contrasted by thorium.

5. CONCLUSION

At present the synchrotron radiation already opened up new possibilities for a wide range of research. The studies are under way which will enable one to change drastically the new technologies.

The rapid development of national programs for the use of SR in various countries proves the importance of this direction which is revolutionary for many branches of science and technology.

REFERENCES

1. G.Schott, Electromagnetic Radiation, Cambridge, Univ.Press, 1912.
2. I.Ya.Pomeranchuk, JETP, 1939, v.9, p.915.
   J. Phys. USSR, 1940, vol.2, p.65.
3. D.D.Ivanenko, I.Ya.Pomeranchuk. DAN SSSR. 1944, vol.44,p. 343. Phys. Rev. 1944, vol.65, p.343.
4. L.A.Artsimovich, I.Ya.Pomeranchuk, JETP,1946,vol.16,p.379.
   J. Phys. USSR, 1945, vol.9, p.267.
5. Schwinger, J. Phys. Rev., 1946, vol.70, p.798.
6. Schwinger, J. Phys. Rev., 1949, vol.75, p.1912.
7. A.A.Sokolov, I.M.Ternov, Synchrotron Radiation, Oxford, Pergamon Press, 1968.
8. G.N.Kulipanov, A.N.Skrinsky, UFN, 1977, vol.2, p.369.
9. H.Winick and S.Doniach, Eds Synchrotron Radiation Research, Plenum, New York, 1979.
10. Handbook on Synchrotron radiation Eds E.E.Koch, 1984,North-Holland, vol. 1.2.
11. Synchrotron Radiation at INP Sib.Div. of the USSR Ac. of Sci. , Bibliography, 1986, Novosibirsk.
12. V.I.Ginzburg, Izv.AN SSSR (phys.ser.) 1947, vol.11,p.165.
13. V.N.Baier, V.M.Katkov, V.M.Strakhovenko, JETP, 1972, vol.

63, p. 2121.
14. D.F.Alferov, Yu.A.Bashmakov, Ye.G.Bessonov, JETP, 1972, vol. 42, p. 1921. Trudy FIAN SSSR, 1975, vol.80, p.100.
15. A.S.Artamonov, L.M.Barkov et al., Nucl.Instr. and Methods, 1980, vol. 177, No 1, p.239.
16. L.R.Elias et al. Phys. Rev. Lett., 1976, vol.36, p.717.
17. N.A.Vinokurov, A.N.Skrinsky, Reprint No 77-69, INP Sib.Div. of the USSR Ac. of Sci., Novosibirsk, 1977.
18. M.Billardon et al., Phys. Rev. Lett., 1983, vol. 51, No 18, p. 1652.
19. X-ray data booklet, 1985, Lawrence Berkeley Lab.
20. Korchuganov V.N. et al., Nucl. Instr. and Meth. 1983, vol. 208, No 1/3, p. 11-18.

FIGURE CAPTIONS

Fig. 1. Synchrotron radiation - geometric scheme, designations.

Fig. 2. Radiation from periodical magnetic structures - geometric scheme.

Fig. 3. Universal functions $\eta(\lambda/\lambda_c)$ and $k(\lambda/\lambda_c)$, determining SR spectral-angular characteristics depending on parameter λ/λ_c.

Fig. 4. Universal function $\nu(\lambda/\lambda_c)$ determining SR angular distribution width at given wave length λ depending on λ/λ_c.

Fig. 5. Dependence of radiation intensity and main polarization characteristics of SR ($I_{\parallel}, I_{\perp}, I, \rho, \varphi$) on vertical angle for values of parameter $\lambda/\lambda_c = 10, 1, 0.1$.

Fig. 6. Averaged over vertical angle linear polarization of radiation at a given wave length as a function of parameter λ/λ_c.

Fig. 7. Universal functions $f_i(K)$ and $q_i(K)$ determining spectral-angular characteristics of harmonics of undulator radiation depending on undulator parameter - K.

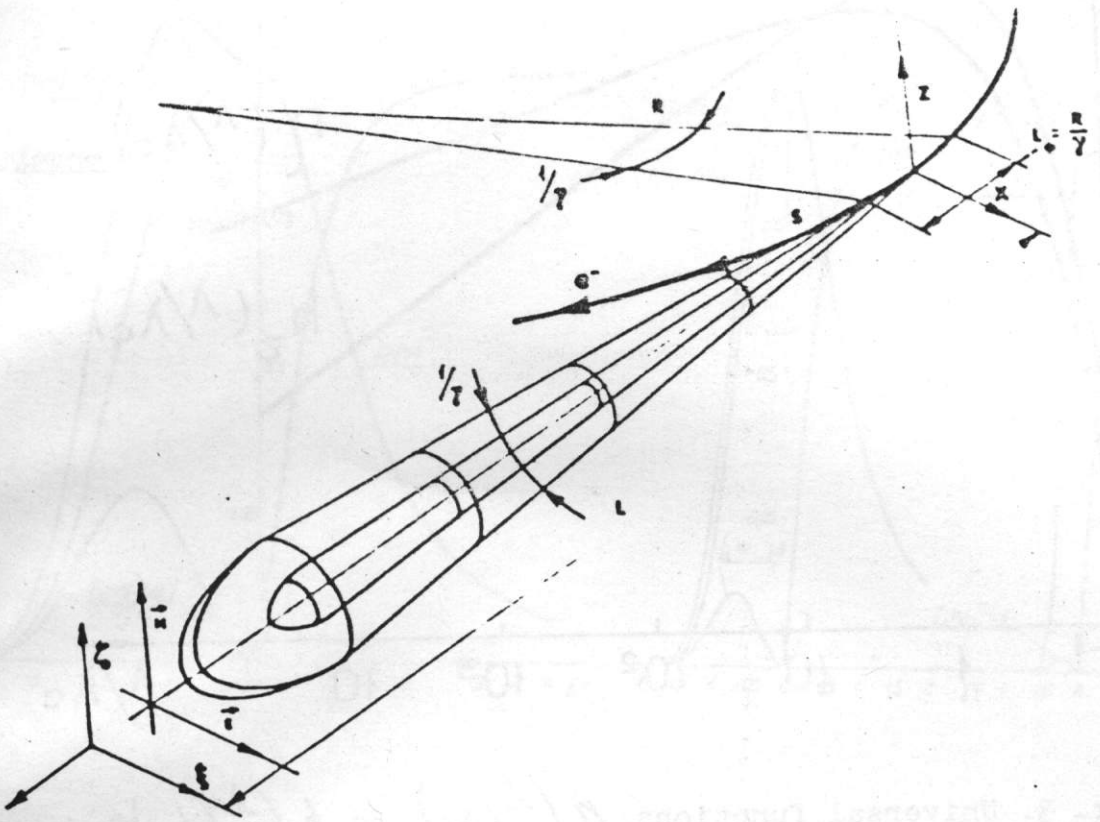

Fig. 1. Synchrotron radiation - geometric scheme, designations.

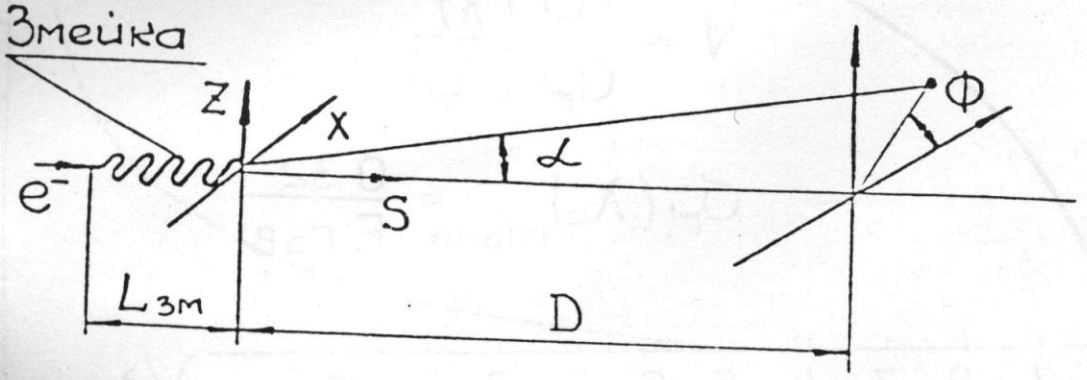

Fig. 2. Radiation from periodical magnetic structures - geometric scheme.

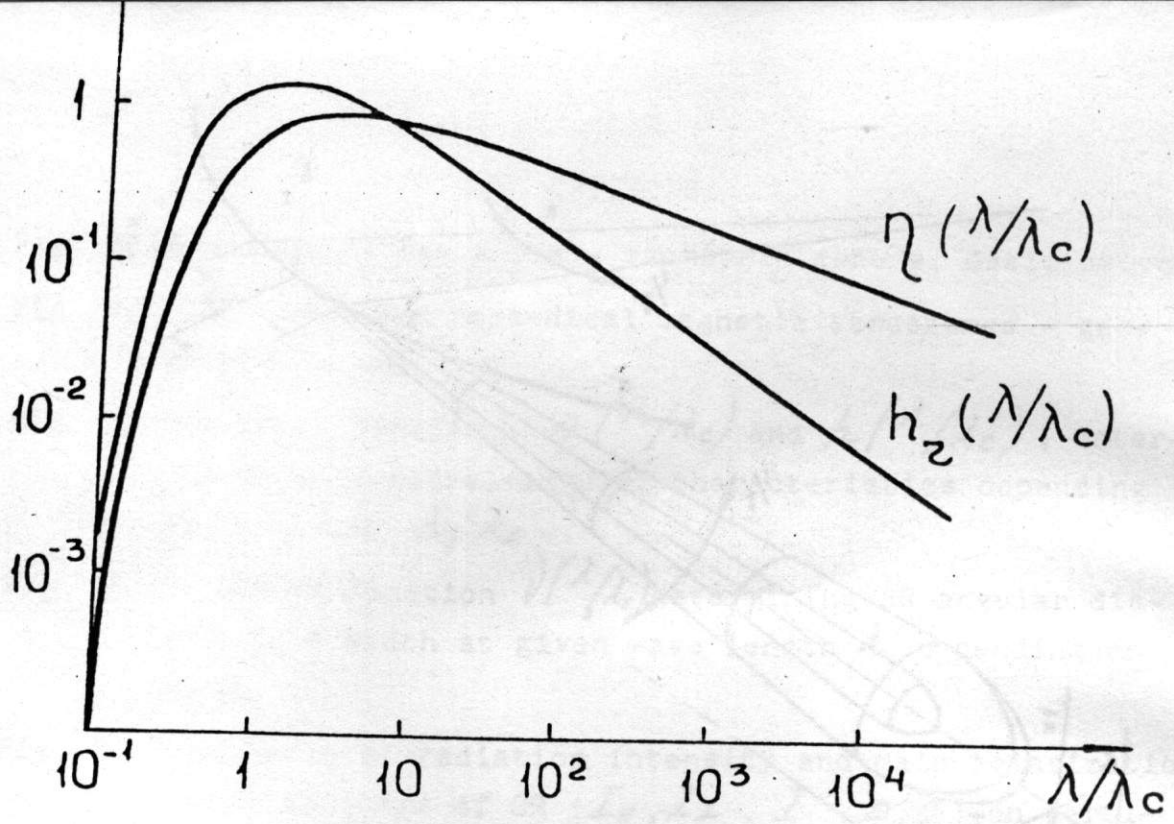

Fig. 3. Universal functions $\eta(\lambda/\lambda_c)$ and $h(\lambda/\lambda_c)$, determining SR spectral-angular characteristics depending on parameter λ/λ_c.

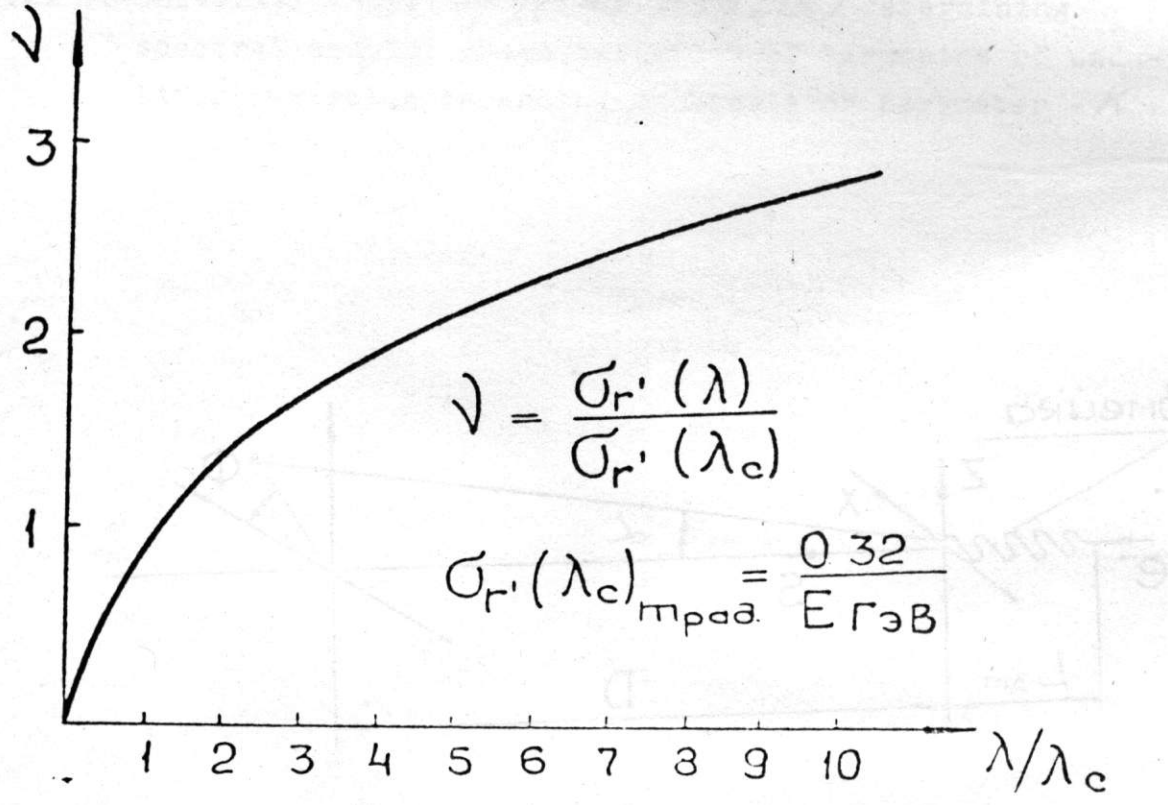

Fig. 4. Universal function $\nu(\lambda/\lambda_c)$ determining SR angular distribution width at given wave length λ depending on λ/λ_c.

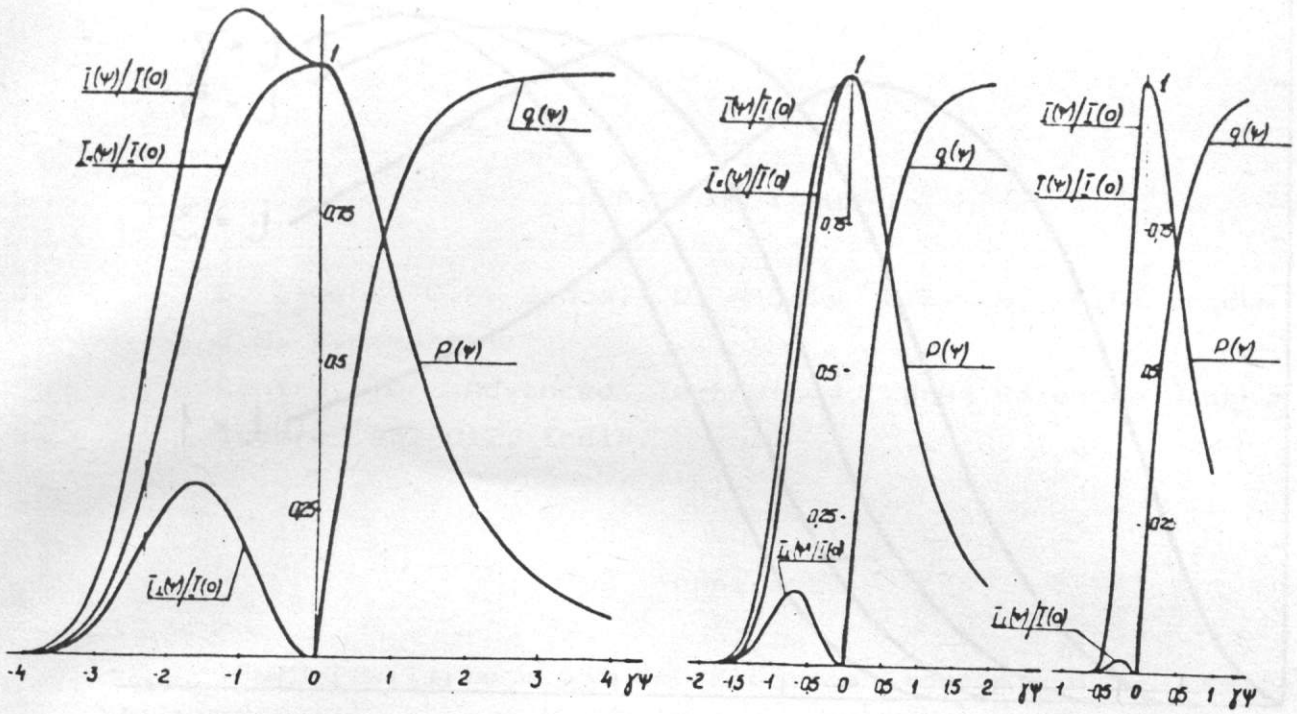

Fig. 5. Dependence of radiation intensity and main polarization characteristics of SR ($I_{\parallel}$, $I_{\perp}$, I, ρ, q) on vertical angle for values of parameter $\lambda/\lambda_c = 10, 1, 0.1$.

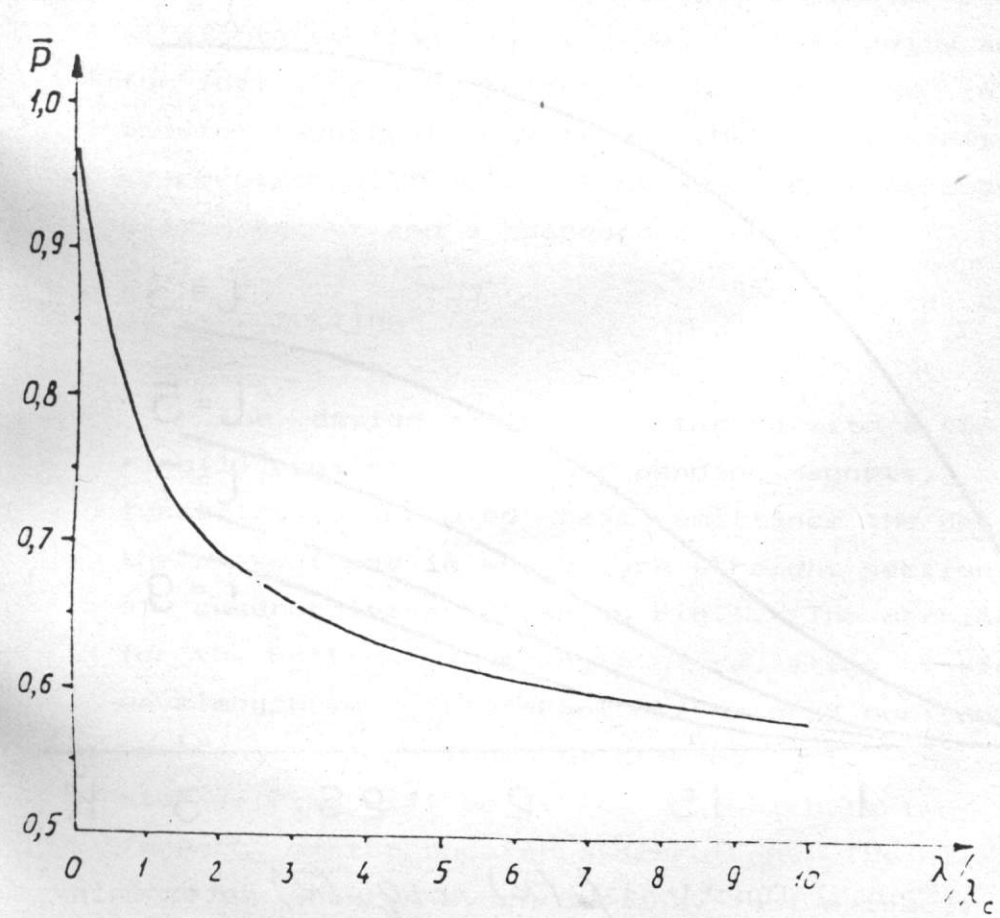

Fig. 6. Averaged over vertical angle linear polarization of radiation at a given wave length as a function of parameter λ/λ_c.

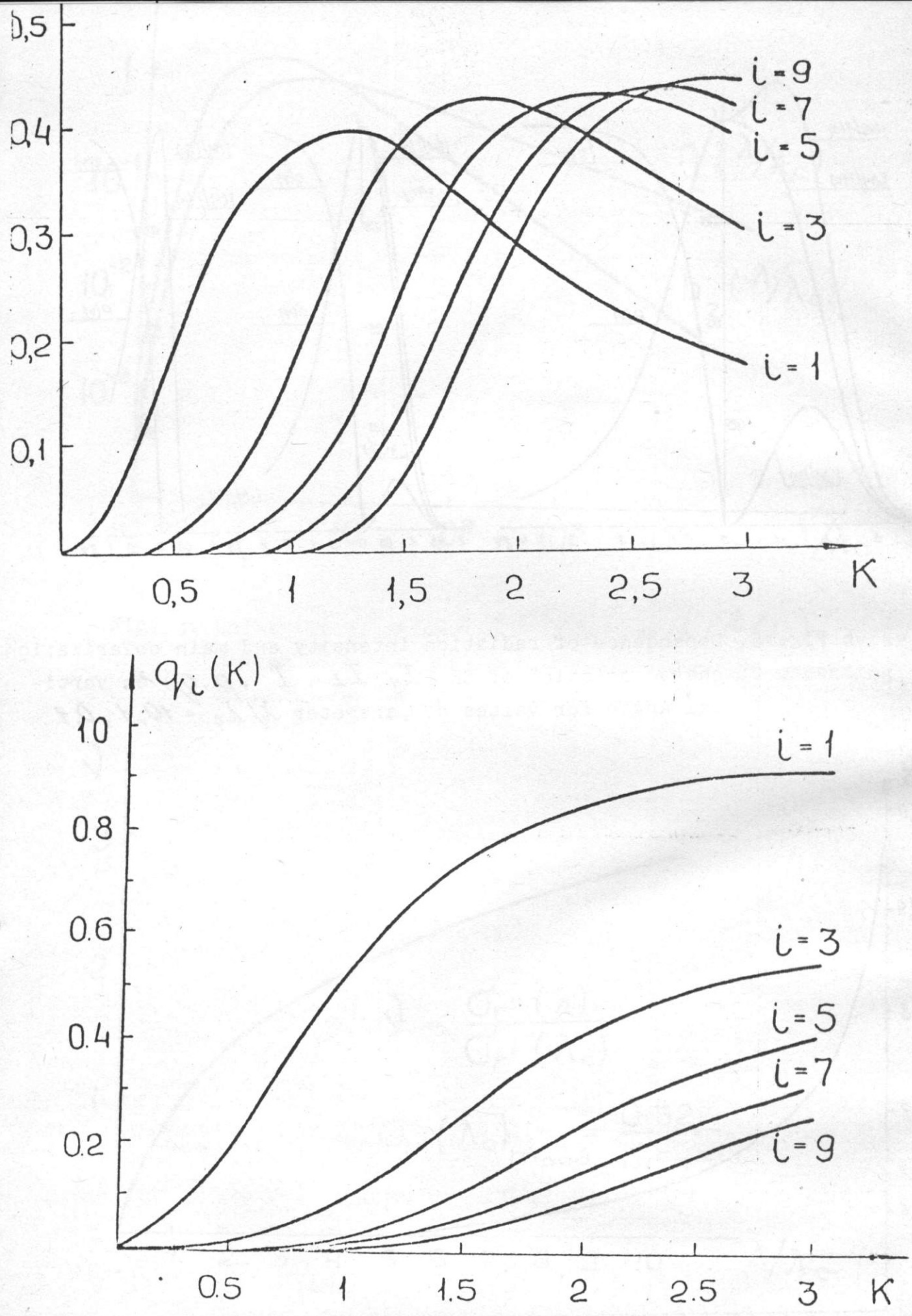

Fig. 7. Universal functions $f_i(K)$ and $q_i(K)$ determining spectral-angular characteristics of harmonics of undulator radiation depending on undulator parameter - K.

OPTIMIZATION OF THE LATTICE OF A STORAGE RING - SR SOURCE

V.N.Korchuganov and E.B.Levichev
Institute of Nuclear Physics, 630090 Novosibirsk, USSR

The possibility to optimize the lattice parameters in dedicated storage rings - SR sources is discussed with a view to reach the best conditions for the extraction of radiation from a magnet, a wiggler, or an undulator. An influence of strong-field wigglers on beam dynamics is considered.

The technique intended to increase the spectral brightness of radiation by minimizing the beam emittance is described and the expressions for minimal emittances of the commonly used lattices are given.

1. INTRODUCTION

Among the requirements specified by experimentors to dedicated SR sources and mainly determining the lattice there are
- an obtaining of a large flux of photons in a wide spectral range (from fractions of an angstrom to several thousands of angstroms);
- generation of SR beams of high spectral brightness.

The first requirement can be met with the use, magnets included, of such insertion devices as wigglers (short-wave spectral range) and undulators (bright beams of VUV and soft X-radiation) for which long straight sections with optimal, for these devices to be mounted, lattice parameters.

The second requirement is identical to an obtaining as low emittance as possible that imposes quite definite constraints on the behaviour of β_x and γ_x in magnets.

Optimization of β_x, β_z and γ_x to achieve the best conditions for SR generation coupled with the requirements characteristic of accelerator physics: flexibility, range of the lattice tuning, necessary dynamic aperture, etc., specify the lattice fairly unambiguously.

2. OPTIMIZATION OF LATTICE PARAMETERS[1]

2.1 Radiation from magnet

For the polarization of SR from bending magnets to be conserved, the divergence of the electron beam in the vertical direction should be less than the natural angular divergence of synchrotron radiation that gives the magnitude of β_z at the point of SR extraction:

$$\beta_z > \varepsilon_z \gamma^2 \qquad (2.1)$$

where ε_z is the vertical emittance and γ is a relativistic factor. The value of β_x is determined by the necessity to minimize the horizontal emittance ε_x.

The dispersion function and its derivative must not greatly contribute to the horizontal size of the beam, because of radial-phase oscillations:

$$\eta_x < \frac{1}{\sigma_{\epsilon/E}} (\varepsilon_x \beta_x)^{1/2} \qquad (2.1.2)$$

$$\eta'_x < \frac{1}{\sigma_{\epsilon/E}} (\varepsilon_x / \beta_x)^{1/2} \qquad (2.1.3)$$

2.2 Undulator radiation

For the generation of high brightness SR beams from an undulator it is necessary that the angular divergence of the electron beam, in the straight section intended for the installation of the undulator, be less than the natural diffraction divergence of the radiation. This gives

$$\beta_{x,z} \gtrsim \frac{\pi \varepsilon_{x,z} \cdot L}{\lambda i} \qquad (2.2.1)$$

where L is the undulator length, λi the wavelength, and i is the radiation harmonic.

This condition has been obtained under the assumption that the energy spread does not contribute to the angular divergence, i.e. η_x = const and η'_x = 0. It is desirable here that the main contribution to the horizontal size of the beam be given by betatron oscillations

$$\eta_x < \frac{1}{\sigma_{\epsilon/E}} (\varepsilon_x \beta_x)^{1/2} \qquad (2.2.2)$$

2.3 Radiation from wiggler

Superconducting wigglers are strong-field devices which are capable of exerting a considerable influence on the basic parameters of a storage ring: emittance, betatron frequencies, etc.

2.3.1 Influence of a superconducting wiggler on beam emittance

It is expedient to install wigglers in special straight sections where both the dispersion function and its derivative are zero throughout the section, i.e. $\eta_x = \eta'_x = 0$. In first approximation, such straight sections do not contribute to the diffusion of the horizontal betatron oscillation amplitudes. On the contrary, due to the fact that the total energy losses caused by radiation increase the radiation damping increases, too, when switching on the wiggler in the region with $\eta_x = \eta'_x = 0$, and this can lead to reducing the emittances as compared with their initial values. For a sinusoidal magnetic field in the wiggler $H = H_0 \sin \frac{\pi S}{d}$, the maximum field H_{max} at which the resulting emittance becomes equal to the initial one (prior to the switching on of the wiggler) may be estimated if the β-functions in the centre of the straight section of the wiggler and in the half-period d of field variation are known:

$$H_{max} \simeq \pi \left(\frac{15}{8}\right)^{1/3} \left(\frac{\mathcal{E}_{x0}}{c_q \gamma^2 / J_x}\right)^{1/3} \frac{H_\rho}{(d^2 \beta_{x0})^{1/3}} \qquad (2.3.1)$$

Here $C_q = \frac{55}{32\sqrt{3}} \cdot \frac{\hbar}{mc} = 3.84 \cdot 10^{-11}$ cm and H_ρ is the lattice rigidity. This expression holds at $\frac{L}{2} \ll \beta_{x0}$, where L is the length of the wiggler.

An obtaining, with as high precision as possible, of the zero dispersion function on the azimuth of the wiggler seems to be extremely important. The value of the uncompensated η_w-function of the storage ring at which, even without regard to the dispersion function in the wiggler, the emittance is equal to the initial one for the wiggler field H_{max}, is estimated from the expression

$$\eta_w \lesssim \left(\frac{\mathcal{E}_{x0}}{c_q \gamma^2 / J_x}\right)^{1/2} \frac{\beta_{x0}^{1/2}}{(H_{max}/H_\rho)^{1/2}} \qquad (2.3.2)$$

It follows from the expression (2.3.1) that when mounting a strong-field wiggler, β_{x0} should be decreased. Meanwhile, according to (2.3.2), a decrease of β_{x0} makes it necessary to minimize the η_w-function, which is not always realizable.

2.3.2 Obtaining a maximum mean brightness of radiation from wiggler

Minimizing the phase volumes of the photon beam produced by a wiggler provided that $\mathcal{E}_z \ll L/\gamma^2$, we can show that the maximum mean brightness is achieved at the following optimal values of β -functions on the wiggler azimuth:

$$\beta_{z_0} = \frac{L}{\sqrt{2}} \tag{2.3.3}$$

$$\beta_{x_0} < \frac{L^2 \alpha_0^2}{2\pi \mathcal{E}_{x_0}} \tag{2.3.4}$$

where L is the wiggler length and $\alpha_0 = K/\gamma$ is the amplitude of the bending angle in the wiggler. As follows from the second inequality, the value of the mean brightness is independent of β_x in a wide range of its values.

2.3.3 Influence of a wiggler on betatron frequencies

The insertion of a wiggler into a storage ring gives rise to a shift of betatron frequencies $\Delta\nu_x$ and $\Delta\nu_z$. For a rectangular-magnets wiggler of length L, with the field $H_z = H_0 \sin \frac{2\pi s}{\lambda_0}$ (λ_0 is the wiggler period) and symmetric about the centre, it is possible to show that the shifts in betatron frequencies are

$$\Delta\nu_x \simeq 0 \tag{2.3.5}$$

$$\Delta\nu_z \approx \frac{1}{4\pi}\left(\frac{H_0}{H\rho}\right)^2 \frac{L}{2}\left(\beta_{z_0} + \frac{L^2}{12\beta_{z_0}}\right) \tag{2.3.6}$$

The shift of $\Delta\nu_z$ is minimal at

$$\beta_{z\,min} = \frac{L}{\sqrt{12}} \tag{2.3.7}$$

The said above makes it possible to summarize that for strong-field wigglers, a straight section is required, where the η_x -function and its derivative are matched to zero, the vertical β_z -function is comparatively small, and the horizontal β_x -function is rather large.

3. EMITTANCE MINIMIZATION

3.1 Conditions for beam emittance minimization

To increase the SR brightness, the emittance of $\mathcal{E}_x$ should be minimized. The general expression for the horizontal emittance of the electron beam in a storage ring, which is determined by quantum fluctuations, is of the form[2]

$$\mathcal{E}_x = \frac{C_q \gamma^2}{J_x} \frac{\oint \mathcal{H} \left|\frac{1}{\rho}\right|^3 ds}{\oint \frac{ds}{\rho^2}} \qquad (3.1.1)$$

where

$$\mathcal{H} = \gamma_x \eta^2 + 2\alpha_x \eta \eta' + \beta_x \eta'^2 \qquad (3.1.2)$$

and α_x, β_x and γ_x are the Twiss parameters of a storage ring.

If the following premises are given:
- bending magnets are the major SR sources,
- bending magnets are all identical and their length is ,
- the behaviour of the β_x, β_z and η functions is the same in all the bending magnets of the ring,

the following known conditions for emittance minimization can be derived: first, the horizontal β_x function should have a minimum on the azimuth of a bending magnet and, second, this minimum should be $S_0 = 3\ell_m/8$ distant from the edge, where $\eta_x = \eta'_x = 0$. Here the minimum value of β_x is equal to

$$\beta_x = \left(\frac{3}{320}\right)^{1/2} \ell_m \simeq 0.097\, \ell_m \qquad (3.1.3)$$

Substituting the expressions for the Twiss parameters into (3.1.2), we obtain an expression for as minimum beam emittance as possible (for the given requirements)[3]

$$\mathcal{E}_{x\,min} = \frac{1}{4\sqrt{15}} \frac{C_q \gamma^2}{J_x} \cdot \varphi_m^3 \qquad (3.1.4)$$

or

$$\mathcal{E}_{x\,min}\,(\text{cm-rad}) = 9.5 \cdot 10^{-6} E^2\,(\text{GeV})\, \varphi_m^3\,(\text{rad}) \qquad (3.1.5)$$

where $C_q = 3.84 \cdot 10^{-11}$ cm, φ_m is the bending angle in a magnet, and $J_x \simeq 1$ is the relative horizontal damping parti-

tion number.

Thus, $\mathcal{E}_{x\min}$ is determined only by the geometric characteristic - the bending angle in dipole magnets forming the achromat.

3.2 Types of the lattices of dedicated SR sources

At present there exist three most frequently used lattices: a Chasman-Green lattice, a triple bend achromat, and a FODO.

No recommendations are available now how to use them in dedicated SR sources, each has both merits and demerits. Sometimes the project considers several lattices simultaneously./4/

3.2.1 Chasman-Green lattice (CG)/5/

The CG comprises two bending magnets and a set of quadrupole lenses to control the behaviour of the lattice parameters (Fig.1). In contrast to the triple bend achromat, the CG periodicity cell has a smaller number of elements and, hence, a larger number of straight sections, with the perimeter being equal. This type of lattice is expected to be used in ESRF, APS and RIKEN.

For the CG that consists of N_p achromatic bends (periods), the minimal emittance is/5/

$$\mathcal{E}_{x\min} = \frac{1}{4\sqrt{15}} \frac{C_q \gamma^2}{J_x} \left(\frac{\sqrt{\pi}}{N_p}\right)^3 \qquad (3.2.1)$$

In fact, this value is 3-4 times greater due to the fact that the optimal β_x and η_x create a considerable chromatism and, as a consequence, this decreases the dynamic aperture, when the chromatism is compensated for.

Besides, in such a lattice, there is no possibility to vary the phase advance of betatron oscillations on the periodicity cell, without a considerable increase of the emittance, and this degrades the flexibility of the lattice./6/

3.2.2 Triple bend achromat (TBA)

Unlike the CG, the periodicity cell in TBA contains an additional magnet and, consequently, it has a lower emittance, with the number of periods being equal (Fig.2). This type of lattice is analysed, for instance, in the projects LBL and SRRC.

The optimized emittance for N_p periods is[5]

$$\mathcal{E}_{x\,min} = \frac{7}{36\sqrt{15}} \cdot \left(\frac{2}{3}\right)^3 \frac{C_q \gamma^2}{J_x} \left(\frac{\sqrt{11}}{N_p}\right)^3 \qquad (3.2.2)$$

As against the CG, an important advantage of such a lattice is, in addition to a smaller emittance, the flexibility and the possibility to vary the advance of the horizontal betatron phase on the periodicity cell (the low emittance remaining the same).[6] However, this lattice is not efficient in respect to the number of straight sections.

3.2.3 FODO[7]

The FODO has found wide application in storage rings for high energy physics (SPEAR, PETRA, PEP); in addition, it is considered in projects DELTA and SLC. It is reasonable to employ the FODO in sources where the SR from bending magnets is mainly utilized because it is a complicated matter to create a great deal of straight sections. Usually, a storage ring - SR source with a FODO is shaped as the racetrack with long straight sections where wigglers or undulators may be mounted.

For the FODO, the optimized emittance is[7]

$$\mathcal{E}_{x\,min} = 4 \frac{C_q \gamma^2}{J_x} \cdot F \cdot \varphi_m^3 \qquad (3.2.3)$$

where φ_m is the bending angle in the cell magnet, and

$$F = \frac{1 - 3/4 \sin^2(\mu_x/2) + 1/60 \sin^4(\mu_x/2)}{\sin^2(\mu_x/2) \cdot \sin \mu_x} \qquad (3.2.4)$$

where μ_x is the horizontal betatron phase advance on the periodicity cell.

For $\mu_x \simeq \frac{3}{4}\pi$, the minimum of $F_{min} \approx 0.62$ is achieved which is rather smooth at $100° \leq \mu_x \leq 160°$ and

$$\mathcal{E}_{x\,min} = 5 \cdot 10^{-11} \gamma^2 \varphi_m^3 \ [\text{cm-rad}] \qquad (3.2.5)$$

References

1 V.N.Korchuganov. Dedicated synchrotron radiation source - storage ring SIBERIA. Ph.D.Thesis. Novosibirsk 1986.

2 M.Sands. The physics of electron storage rings. An introduction. SLAC-121. UC-28 (ACC).

3 V.N.Korchuganov et al. Optimization of the parameters of the dedicated synchrotron radiation source for technology. NIM 208 (1983) 11-18.

4 7 GeV Advanced Photon Source. Conceptual Design Report, Argonne, ANL-87-15, 1987.

5 A.Wrulich et al. Workshop on Lattice Comparison for the ESRF. ESRF_SR/LAT-86-19

6 A.Jackson. A comparison of the Chasman-Green and Triple Bend Achromat Lattices. LBL-21279, 1986.

7 H.Wiedemann. Brightness of Synchrotron Radiation from Electron Storage Rings. SLAC-PUB-2342, 1979.

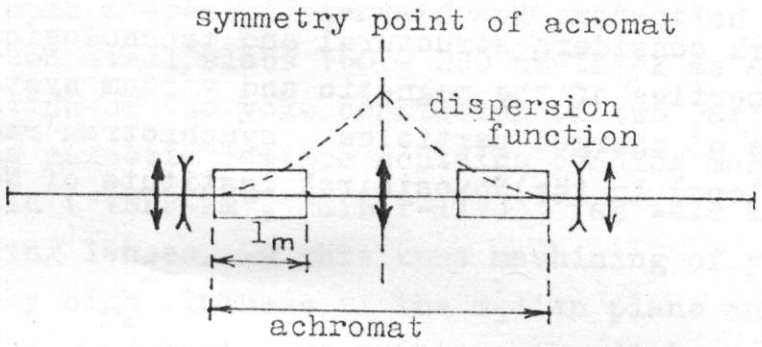

Fig.1. Basic CG lattice.

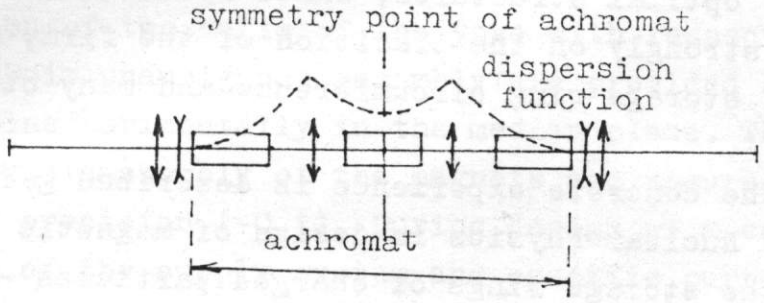

Fig.2. Basic TBA lattice.

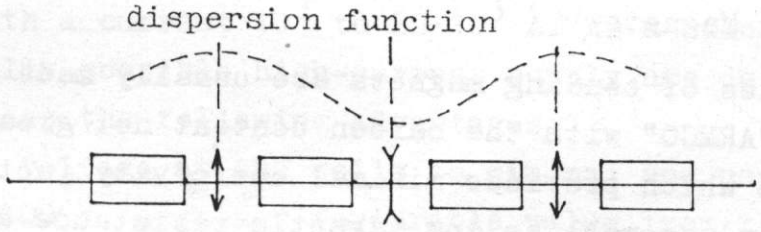

Fig.3. FODO structure.

ENGINEERING ASPECTS OF SRS

E.M. Trakhtenberg
Institute of Nuclear Physics,
Siberian Division of the USSR
Academy of Sciences

This work considers structural and technological characteristic properties of the magnetic and vacuum systems of the storage rings of charged particles - synchrotron radiation sources developed in the Novosibirsk Institute of Nuclear Physics.

INTRODUCTION

During recent years more and more storage rings of charged particles have been created as specialized synchrotron radiation sources. Various engineering approaches are used in the construction of such devices. It is difficult to create "absolutely" optimal structures, since specific design approaches depend strongly on the tradition of the firm, technology it is using, storage ring circumference and many other parameters.

Below the concrete experience is described gained at the Institute of Nuclear Physics in design of magnetic and vacuum systems of the storage rings of charged particles - synchrotron radiation sources.

1. ELEMENTS OF MAGNETIC SYSTEMS

1.1. Bending Magnets

The yokes of bending magnets are usually made of steel similar to "ARMCO" with the carbon content not greater than 0.03 - 0.04% which provides minimal coercivity (not greater than 0.1 A/cm) as well as low magnetic resistance at high field values. To decrease a radius of bending magnets high enough values of the magnetic fields are used (1.5 - 1.8 T). The highest value of the operating magnetic field of 2.3 T has been achieved at the "BEP" storage ring[1] using a special magnet design with a large pole width and relief chamfers much larger than usual. In our opinion laminated yokes produced of exactly stamped plates of low-carbon steel are more expensive, especially for storage rings at the energy 0.5 to 2.5 GeV with high enough value of $\Delta R/R$, where ΔR is a po-

le width and R is a radius of an equilibrium orbit. To make the production of such magnets simpler and cheaper, our Institute in collaboration with the Magnitogorsk Metallurgical Plant developed a special standard and production technology for low-carbon steel slabs 160 - 280 mm thick as a rule allowing production of the yoke consisting of two parts only. Usually, the magnetic lattice contains bending magnets with a plane field ("VEPP-2M", "Sibir-II")[1] as well as focusing and defocusing lenses. In this case machining of yoke pieces requires only high flatness of the median plane and the pole (0.03 - 0.05). One must also maintain the distance between them with an accuracy of ± 0.03 which is technically possible and can be achieved at a turning-table machine tool. Preliminary machining of the base planes of the magnet can be performed with a mentioned above accuracy at any equipment.

Fixation of two halfs of the yoke with respect to each other and their unambiguous assembly are provided by placing two-three pins horizontally in the median plane. This makes assembly and disassembly of the magnets and ensures necessary assembly precision (~ 0.1). During design of a coil if allowed power of the supply system and specific current density are chosen, one can widely vary the number of wires and the current in them, i.e. Jw = const.

The experience of our Institute covers constructions of windings with a current 10^3 to $20 \cdot 10^3$ A. As a rule, coils with maximally possible high-current supply are designed which provides the following advantages:

1. The voltage at the coils is minimal and usually does not exceed 100 V, a rather favourable value from the security point.

2. The small number of wires at the high-current supply and, correspondingly, a smaller total length of the coil allow coil cooling with one water input and output. This considerably simplifies the coil design, makes its cost lower and its reliability higher.

3. Taking into account a space factor (a thickness of insulation interlayers) the cross-section of the high-current coils is slightly smaller than that of the low-current one.

A main disadvantage of high-current coils is significant power losses in the joints and necessity of their careful construction. The number of bolts and their size are chosen so that a specific pressure on the joint area is not less than 2000 N/cm^2. One should provide high flatness and cleanness of the joints. It is recommended to electrographically cover a joint with silver. The resulting coating is more firm than that after the galvanic coating. Even after the careful joint preparation it is difficult to obtain a contact resistance less than 10^{-6} Ohm (at low resistance and $J = 10^4$ A the power of 100 W is released in each joint).

The coils of the bending magnets are usually manufactured of copper bus with a square or rectangular section. Joint and lead connections are made by soldering using a silver solder PSr-45 (45% of Ag, 25% of Zn, 30% of Cu) through adapter plugs. It is recommended to strengthen joints by screws and expand a surface area of soldering. Application of expensive silver solder can be justified by its high technological quality: good fluidity, wettability, high mechanical firmness and low sensitivity to small deviations from the temperature regime of soldering.

Interturn and interlayer insulation is performed with strips of glass-cloth-base laminate with a removed lacquer layer. Its thickness is usually 1 mm, two strips 0.5 mm thick are placed parallelly to provide the overlapping of joints.

The characteristic property of the coil design is that the commutation is in the middle of the coil and the current leads come to an inner radius of the magnet through the cut in the yoke. This allows completely symmetric ends of the magnet. Another point is that the sites of the coil commutation appear in the convenient place which does not have other elements.

The isolation of the case of the coil is done with surgical tape or glass tape afterwards impregnated with epoxy in a form under a pressure of 4 - 6 atmospheres with vacuum preprocessing of both a form and an epoxy volume. Such a design allows stable coil size, good insulation quality during long-term operation (10 - 15 years and more), high mechanical firmness and good appearance. A coil constructed in such

a way is installed on the magnet pole with high precision, so that no additional fixation but wedging out on the pole is used in some storage rings.

1.2. Dipole and Quadrupole Lenses

The main problem while making dipole and quadrupole lenses is machining of the pole surface of a special shape. After comparing different methods we have chosen machining with an accurate forming cutting tool at the planing-machine.

This method allows machining of exact profiles of different shape with a deviation from theoretical size not larger than ± 0.03. The length of such a pole can be as large as 1 m.

Figure 2 shows such a forming cutting tool. Its characteristic property is two mutually perpendicular base planes with respect to which its profile is made. A possible accuracy of the profile with respect to the bases is ± 0.01. The profile can be described in arbitrary form (by formula, by a coordinate table) and can be an arbitrary curve. For example, compensation of quadratic and cubic nonlinearities can be introduced in the hyperbolic profile and so on.

Machining with such a cutting tool and a way of mutual fixation of the tool and the machined piece are shown in Fig. 3, whereas Figure 4 demonstrates a simple method of controle using a special gauge and a set of probes.

2. ELEMENTS OF VACUUM SYSTEMS

One of the main problems while constructing storage rings used as synchrotron radiation sources is that of reliable superhigh vacuum (10^{-7} - 10^{-9} Pa) in the beam pipe. The situation is additionally complicated by that this vacuum should be obtained under intensive gas release stimulated by synchrotron radiation of the electrons (positrons) rotating in the storage ring. The level of such a stimulated desorption is 5 - 10 times higher than thermal gas release from the walls of the beam pipe[3]. Specific power densities in modern storage rings can be higher than 100 W per cm in a regular structure. This requires special intensively cooled radiation absorbers inside the beam pipe. It is thus evident that the large number of electrophysical devices placed inside the

pipe as well as the necessity of baking the pipe up to 250° - 300° make the structuring of the beam pipe a rather complicated problem.

2.1. Use of Welding for Beam Pipe Manufacturing

For the first time a wide-scale experiment on the use of welding for beam pipe manufacturing was performed in 1971 during the construction of the VEPP-2M collider[3], when about 500 m of welded joints were made. The experience of 15 year operation showed high reliability of the decisions concerning welding constructions and the technology of their performance.

We shall refer to the welded joint as vacuum-sealed if helium leak detector with a sensitivity of $1 \cdot 10^{-8}$ l·Pa/sec does not discover leak. The main point of our design and technological conception is maximum reliability of operation under periodical bakings.

Relatively small design complications of the connected elements, such as levelling of wall thickness, designing thermal isolation, facets, preparation, technological ledges are almost always advantageous. They slightly increase the cost of mechanical machining, but the reliability of welding becomes higher.

Centering, use of pins, other ways of unambiguous mutual orientation in connection sites justify additional mechanical machining under conditions of single or low quantity production, because even the simplest gadgets are usually more expensive than additional operations.

Some examples of the design decisions for high-vacuum baked welded joints are presented in Fig. 5.

The main method of obtaining such joints is welding by a non-melting electrode in inert gas environment (argon or helium).

Tungsten alloyed with lanthanum or ittrium is used as a non-melting electrode. Helium is applied when an increased specific power of an arc is necessary, i.e for welding materials with high heat conductivity (copper, aluminium).

Two most commonly used ways of making such joints are melting of edges of connected pieces in the welding site (IN) or application of a wire from the same material as an additi-

ve (INw). In the first case the joint leg should not exceed 1.5 mm.

Vacuum-sealed welding of copper and stainless steel requires strict design rules shown in Fig. 6.

One of the main parameters of vacuum-sealed welded joints is the depth of a welding joint. Our experience shows that the following depths can be obtained:

IN from one side - not larger than 1.5 mm

IN from two sides - not larger than 3 mm

INw from one side (without edge preparation) - not larger than 2 mm

INw from two sides (without edge preparation) - not larger than 4 mm

INw from one side (with edge preparation) - not larger than 6 mm

INw from two sides (with edge preparation) - not larger than 10 mm.

One should keep in mind that the depth must be in the range (0.3-0.8)s, where s is a thickness of the thinnest connected elements in the welding site. Lower thickness results in breaking vacuum density because of residual tension in a joint even at small load during operation, whereas a higher one causes significant deformations, large internal tension and makes welding more expensive.

Our practical experience has shown that IN can be recommended as the best welding method for described problems if metal pieces with a thickness 0.8 to 5 mm are constructed without additional strengthening of the joint zone by clamps. If such strengthening is possible, welded elements can be up to 10 mm thick.

Special attention should be paid to the design of the places where joints intersect. To make such connections more reliable intermediate machining is needed. For example, a box of four plates before welding two end flanges must be machined to remove defects possible at the joint outlets. The recommended allowance for machining is 2 - 4 mm depending on the size and thickness. One should remember that vacuum-sealed joints should not be machined after welding. If, nevertheless, it is needed, joints welded several times should be

used.

The question often arises about a side of joints of vacuum-sealed baked connections. Many authors believe that the inner side should be used to avoid voids and pockets facing the vacuum volume. However, if a large electrophysical installation is considered which has a lot of joints access to which is difficult, and also if its disassembly is complicated and time-consuming, we strongly recommend using the external side. We believe that reliability in operation and the capability of easy repairing are most important. In fact, leakage in the external joints can easily be found and removed by additional welding or filling them up with high temperature silicone laquers. Modern methods of preparing vacuum units such as boiling in distillate, ultrasound cleaning, vacuum baking at temperatures up to 400 - 450° allow good cleaning of the voids facing the pumped volume.

Often defects are found in high-vacuum baked pieces due to the leakage in the bulk. Dangerous in this respect are the walls 3 - 4 mm or smaller thick, especially in the pieces with complicated configuration in which fibres are cut during machining. Most frequent is the leakage along the fibres (direction of rolling), especially when round material has been used. Sheet rolling, tubes and special profiles are much more firm. Such defects usually appear after the ready product is baked. The following methods to suppress such leaks are recommended:

1. For pieces with thin walls the direction of rolling must be indicated in the drawings, so that thin walls are along this direction.

2. In fabrication of the pieces with a complicated configuration more frequently use forging or welding of several workpieces of the sheet material.

3. Fabricate thin wall pieces from the sheet material, even if it seems technologically unprofitable.

4. Check workpieces machined beforehand to detect leak in the bulk with their preliminary baking in the vacuum oven up to 400° - 450° during at least 4 hours and reject defective.

5. Galvanically cover thin walls in pieces made of rod material with copper 10 - 15 μm thick with subsequent annea-

ling of this coating in the vacuum oven at 800° - 850°.

The latter operation was initially used to repair defective products, but because of its relatively small cost and simplicity it is widely used preventively.

The most radical method consists in using vacuum arc remelting for important pieces with thin walls of stainless steel.

In the high-vacuum baked units developed in the Institute since 1970 for demountable joint packings welded flange connections are widely used (Fig. 7) with an easily filed edge 0.8 - 1 mm thick. The welding depth for such flanges must not exceed 0.8 - 1 mm.

If leakage appears in such joints after baking it can easily be located and removed by additional welding without spoiling vacuum or closed with laquer.

If such a connection should be dismounted which happens rather seldom in baked high-vacuum system, a joint is filed or removed by some tools. The time needed to file a flange with a diameter of 100 mm does not usually exceed 30 - 40 minutes which does not differ much from the time of careful groove-wedge connection mounting.

Such a design of the joint connections is used both as flat and cylindrical flanges. A maximum diameter of such a connection was 1200 mm, the size of a thin part of the flange is usually 5 to 10 mm providing 4 - 8 dismountings. If a larger number of dismountings is needed, a joint connection with an adapter (Fig. 7c) is used. In some cases flanges are replaced after many-year operation.

Dismountable seals of the "Couflat" type are used for connecting ceramic glass leads or other units which can possibly be defective.

2.2. Specific Features of Vacuum Soldering

For baked elements of the high-vacuum electrophysical installations vacuum soldering is appropriate. Main advantages of this method are listed below.

1. Heating in the vacuum oven is uniform. This, as well as slow cooling of the product together with an oven, results in small shifts of the product size.

2. Soldering is combined with the outgassing annealing of the product.

3. No oxides are produced on the oven. This allows to avoid additional mechanical machining after soldering.

4. Vacuum soldering is fluxless so that the quality of the soldered joints is much higher.

5. When heated to the soldering temperature in vacuum, the connected surfaces are chemically clean. A solder spreads easily over minimal capillary gaps also resulting in higher quality and reliability of the soldered connections.

Heating during vacuum soldering is performed either in vacuum ovens or in vacuum volumes by electron bombardment from the ring cathodes made of tantalum or tungsten. A heated piece is placed inside. A necessary condition for obtaining a reliable soldered connection is to use technological walls or chamfers for solder supply and in some cases grooves for placing solder. Some of the decisions are presented in Fig. 8. One should provide the unambiguity of the mutual orientation of connected pieces. To this end pins, centering, grooves or special conductors are used. One should remember that they must be created from the materials with the same coefficient of linear expansion as that of the soldered pieces. One should not forget some elements (for example, graphite spacers) which would prevent from soldering or welding of the conductor to the connected pieces.

The size of the gap between soldered elements at the soldering temperature must be 0.05 - 0.1 mm. If different metals are soldered, the allowance for the gap must take into account the difference between the coefficients of linear expansion. If above mentioned capillary gaps are impossible, for example, because of the large size of the soldered pieces, the main soldered joint should be made over the plane using a foil of solder or corresponding coating of the connected surfaces. One of the types of the vacuum soldering is contact-reactive soldering with silver coating.

One must keep in mind that silver solder should not be used for steel 12Х18Н10Т both in uniform combination or those of different types on the boundary between water and vacuum. Such a connection will be destroyed after some years

because of the electrochemical corrosion along the boundary between stainless steel and silversolder. The destruction time becomes smaller if the corrosion medium gets more active, at higher temperatures or radiation. If such connections can not be avoided, they must be designed in such a way that a silver solder had no contact with stainless steel. For example, one can beforehand melt copper inside the workpiece of steel 12X18H10T in vacuum and then perform soldering of copper with copper using silver. Such a technology has been first applied to radiation absorbers of the VEPP-2M beam pipe and passed successful check during more than 15 years of operation.

Finally, as another example of successful vacuum soldering one can mention the high-current coil of quadrupole lenses for the BEP storage ring in which 34 joints have been simultaneously soldered in one section of the coil. 30 such sections were made. A current of 9000 A and a channel for water cooling pass through each joint.

2.3. Use of Aluminium Alloys for Beam Pipes

During last years special aluminium profiles obtained by hot extrusion have been used abroad for beam pipes of electron storage rings. Since 1984 our Institute in collaboration with the Moscow Institute of Light Alloys constructs profiles of different shape and successfully uses them as workpieces for beam pipes[4]. An aluminium alloy AMtS has been experimentally verified which showed some advantages compared to stainless steel:

1. Beam pipes obtained by extrusion from this material allow a radiation absorber to be installed directly in the beam pipe wall as well as provide the constant cross section of the pipe throughout the whole circumference.

2. The heatconductivity coefficient of this alloy is 8 times higher than that of stainless steel, so that scattered synchrotron radiation does not cause local overheating of the beam pipe. It also allows a convenient baking of the beam pipe to be performed after its thermal outgassing after assembly.

3. Aluminium and its alloys possess extremely low coef-

ficients of thermal desorption. After chemical cleaning and heating at 200°C gas release of the AMtS alloy is $2 \cdot 10^{-11}$ l·Pa·sec^{-1}·cm^{-2}. For stainless steel 12X18H10T chemically cleaned and outgassed at 450°C gas release is $4 \cdot 10^{-11}$ l·Pa·sec^{-1}·cm^{-2}.

4. Aluminium alloys have a coefficients of electron stimulated desorption a factor 2 - 3 lower than that of stainless steel.

5. The cost of beam pipes extruded from aluminium alloys is much lower than that produced of stainless steel even taking into account the cost of special equipment.

Vacuum systems of the storage rings in which pipes extruded from aluminium alloys are used also have pumping and diagnostics units. These units are boxes of stainless steel in which radiation absorbers, different measuring and diagnostic equipment are installed as well as lumped pumps for preliminary and final pumping.

Connection of the stainless cases of such units to aluminium beam pipes is performed through bimetallic flanges-adapters 12X18H10T + AMtS. Such a bimetal can be produced by hot rolling, and adapters made of it have passed serious tests for the vacuum density of the joint during a long time. The tests consisted of three stages and included thermal cycle (heating, cooling), thermal shock (heating up to 450°C and sharp cooling in cold water) and multiple heating (holding at 450°C during 100 hours). All these tests confirmed the high reliability of the bimetal thus produced.

It is not difficult from the technological point of view to obtain a necessary radius corresponding to the orbit radius using extruded workpieces of the beam pipes.

It should be mentioned, however, that up to now we failed to obtain a wall thickness less than 3-4 mm in such an aluminium pipe depending on the pipe section. It is higher than that needed to keep atmosphere pressure.

One can not make a wall thickness lower both by technological reasons and because of that for reliable welding of the pipe with a flange-adapter such a wall size is needed. This results in slight increase of inter-pole gaps in magnets and lenses of the storage ring and corresponding increase of the power supply by 8 - 10%.

REFERENCES

1. V.V. Anashin, I.B. Vasserman et al., "Electron-positron Storage Ring BEP, Proceedings of the IX All-Union Meeting on Accelerators of Charged Particles (in Russian), Dubna, 1985, v. II.
2. N.A. Kuznetsov, E.M. Trakhtenberg, "Machining of the Poles in Magnetic Systems of Accelerators and Storage Rings Using Forming Cutting Tool", Preprint INP 70-73, Novosibirsk, 1970.
3. V.V. Anashin, G.I. Kulipanov et al., "Storage Rings VEPP-2M and VEPP-3 as Synchrotron Radiation Sources". Proceedings of the V All-Union Meeting on Accelerators of Charged Particles (in Russian), Moscow, 1977.
4. V.V. Anashin, N.G. Gavrilov et al., "Vacuum System of the Special-Purpose Synchrotron Radiation Source - Storage Ring Sibir-II", Preprint INP 88-109, Novosibirsk, 1988.

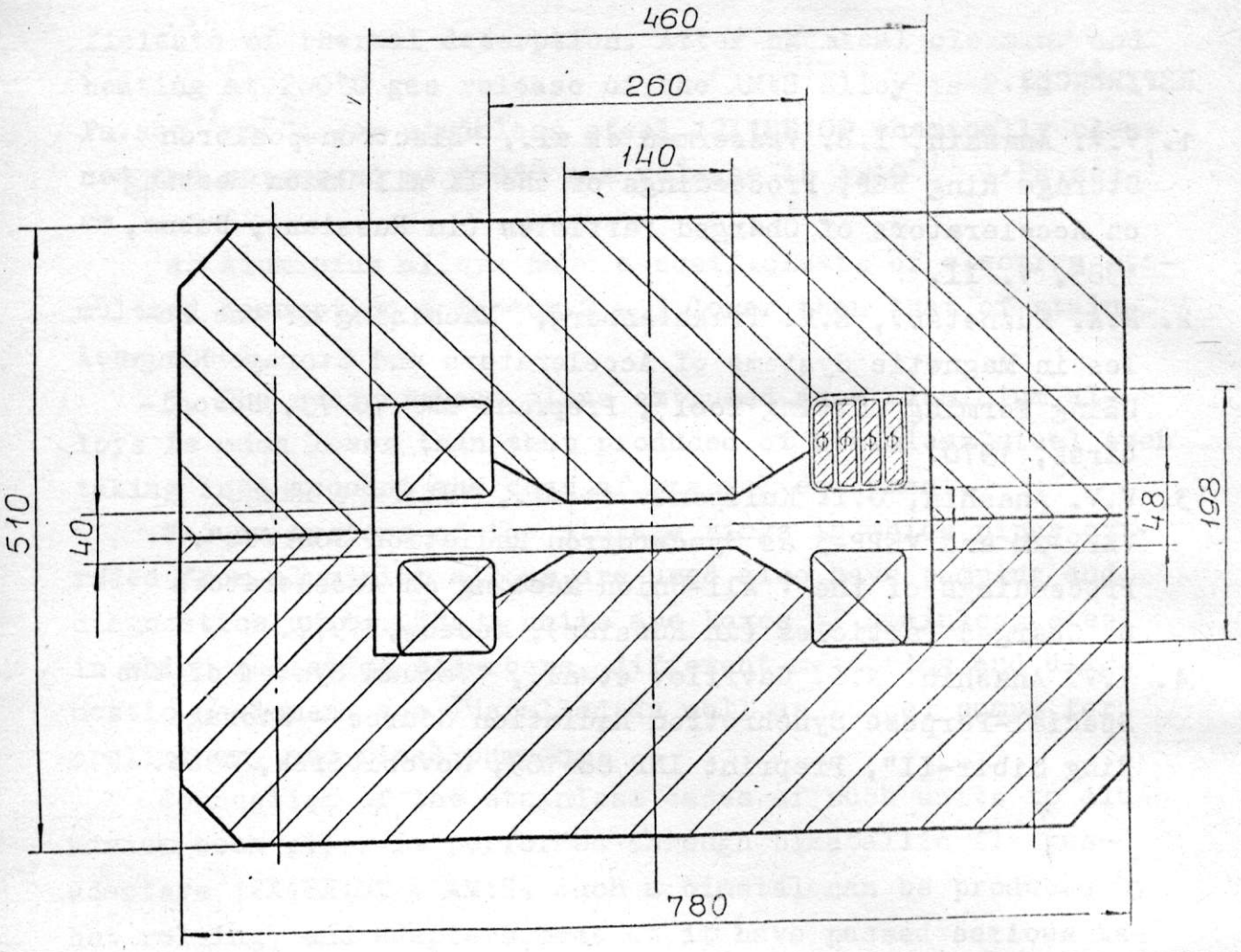

Fig.1

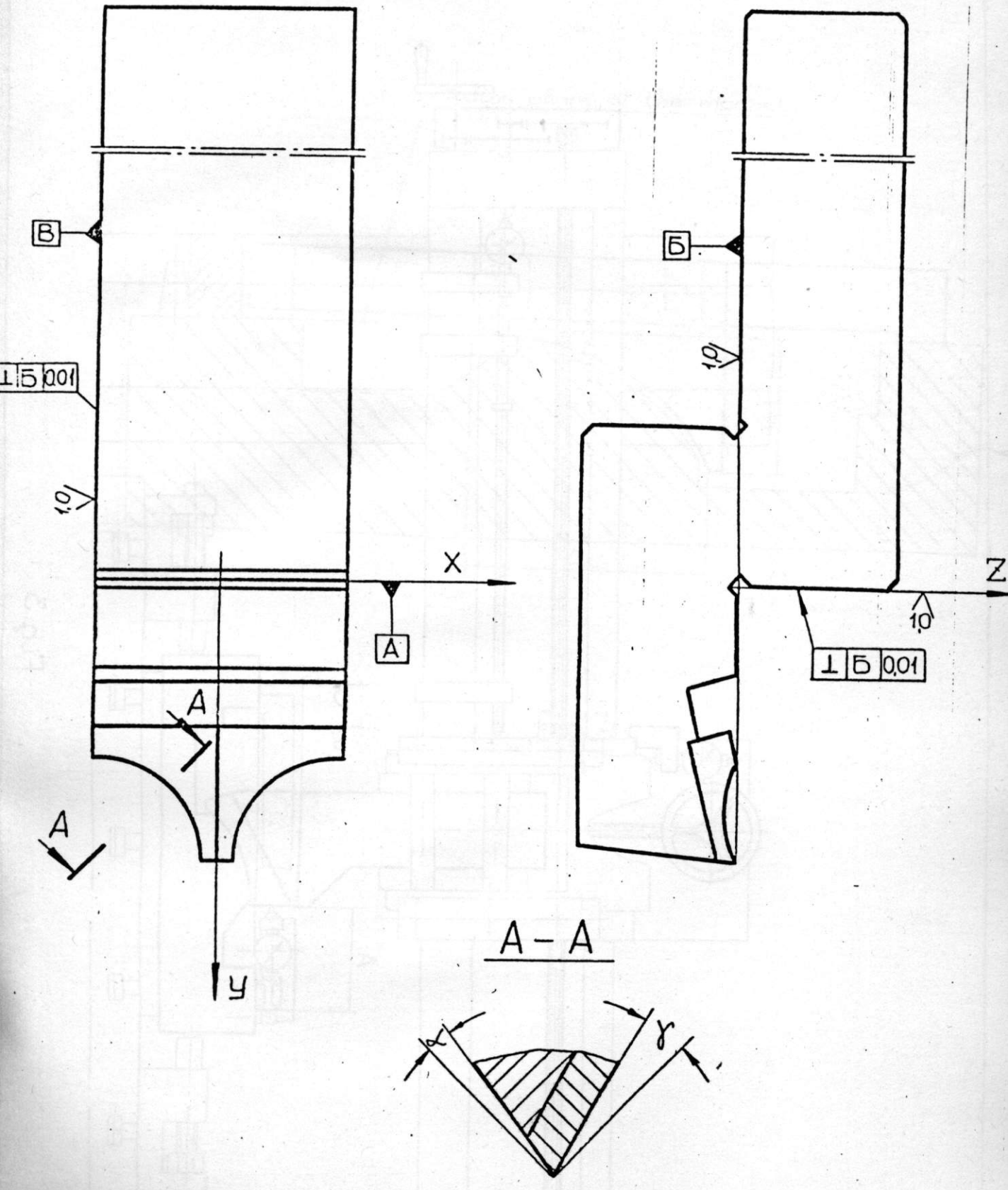

Fig. 2

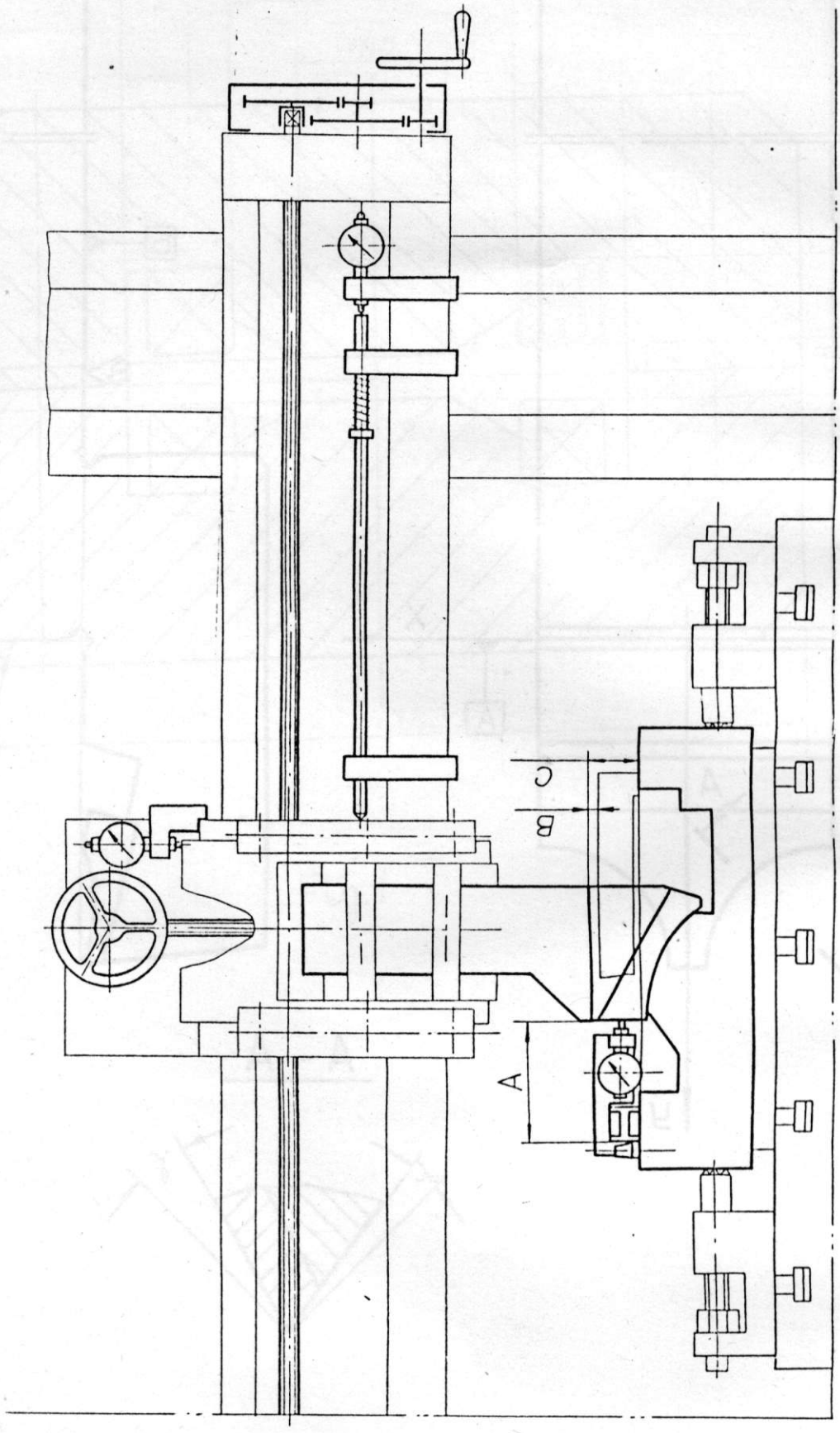

Fig.3

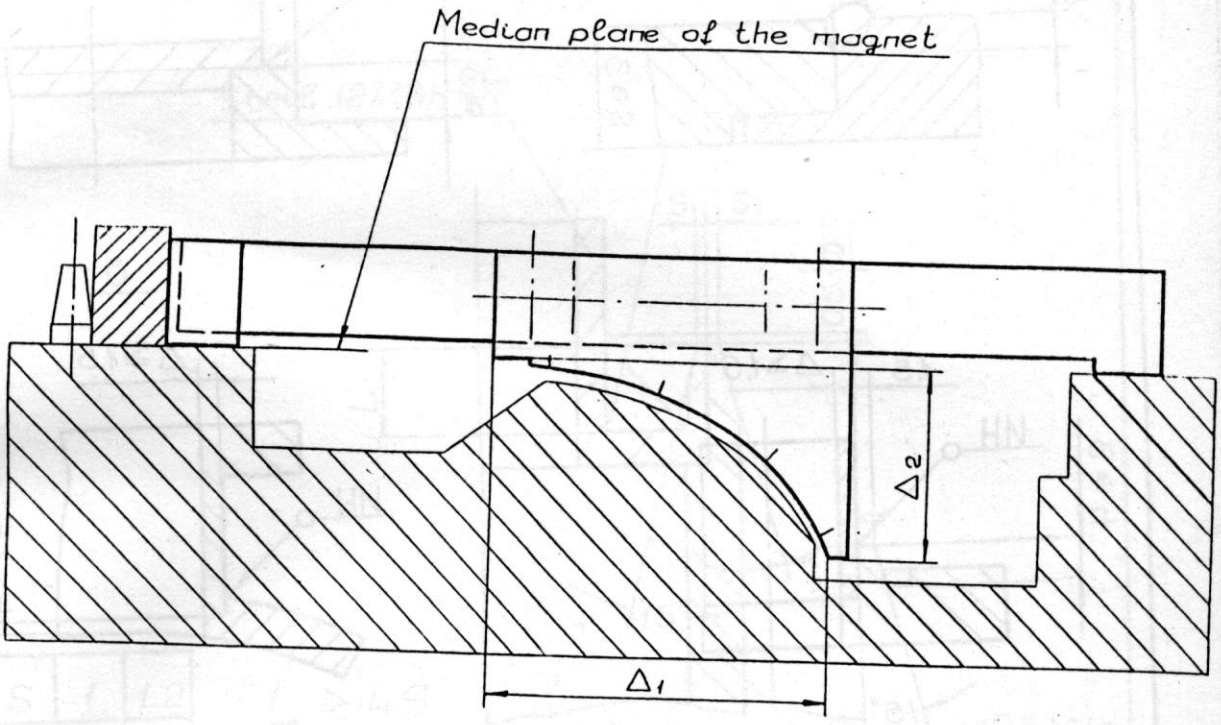

Fig. 4

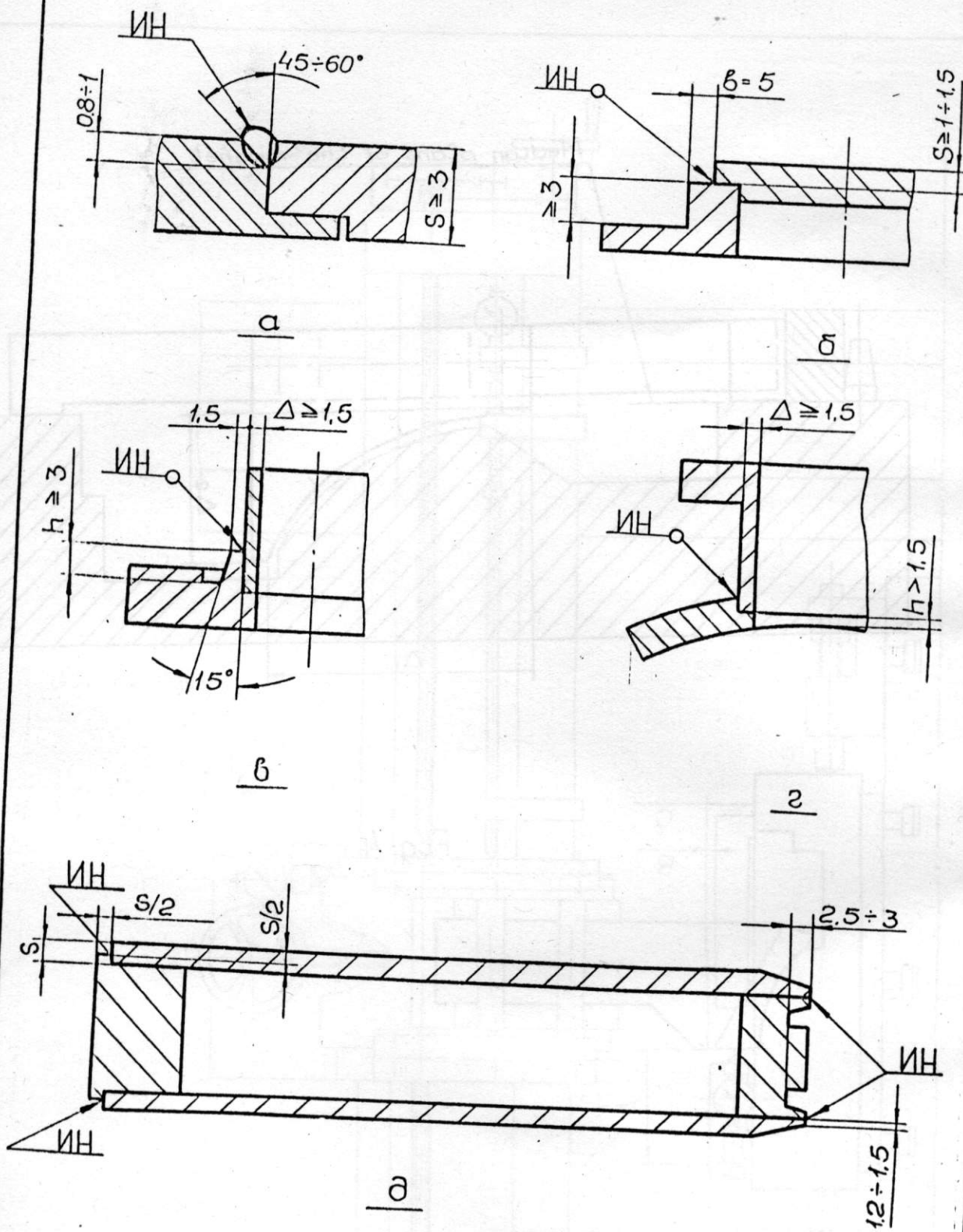
ИН
45÷60°
0,8÷1
S≥3
а
ИН
в=5
S≥1÷1,5
≥3
б
1,5
Δ≥1,5
ИН
h≥3
15°
в
Δ≥1,5
ИН
h>1,5
г
ИН
S/2
S/2
S1
2,5÷3
ИН
ИН
1,2÷1,5
д

Fig. 5

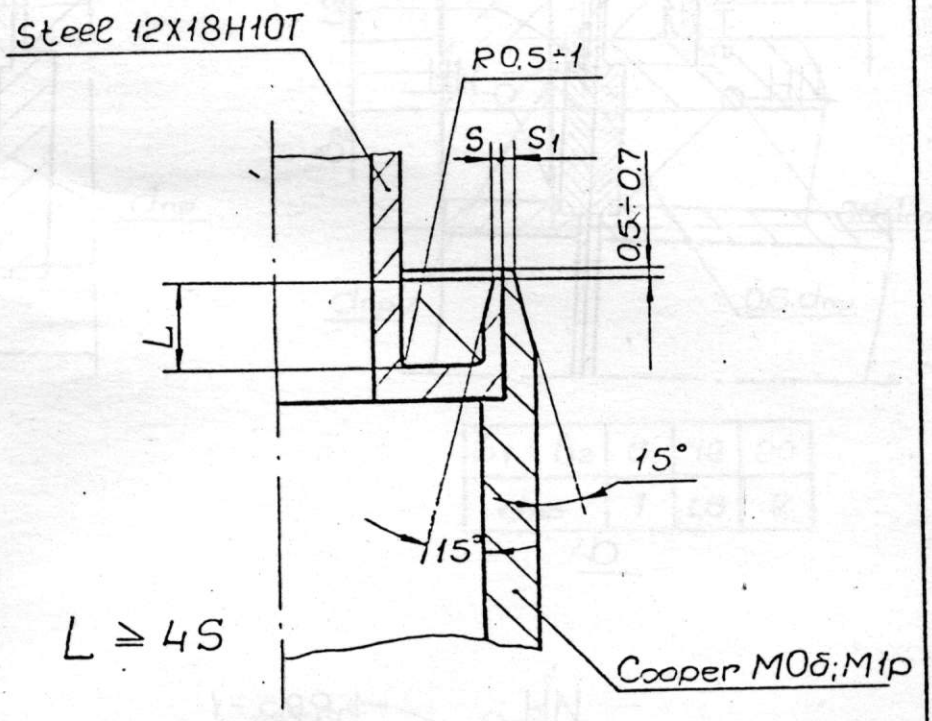

S	1	1.2
S1	0.8	1

$L \geq 4S$

Fig. 6

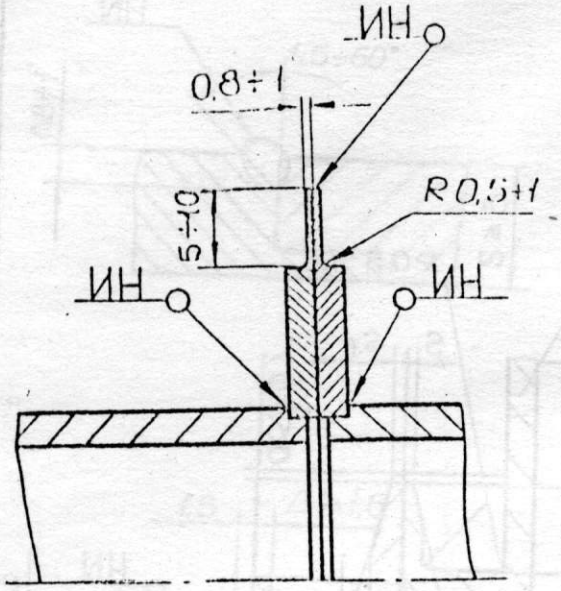

а

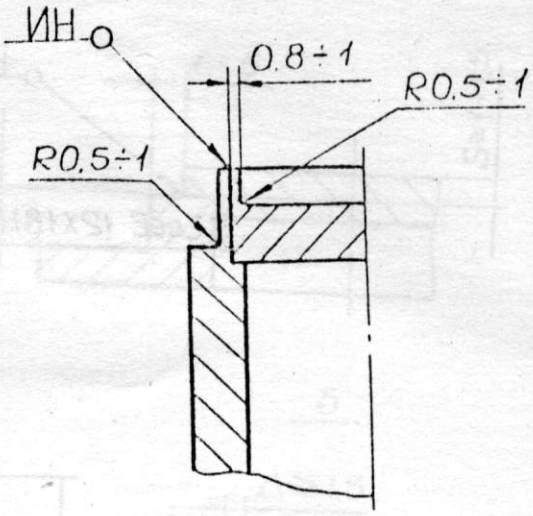

б

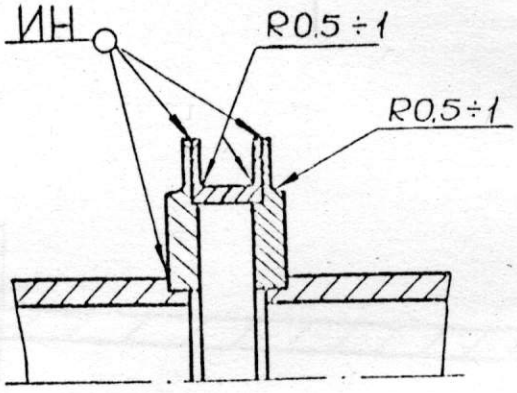

в

Fig.7

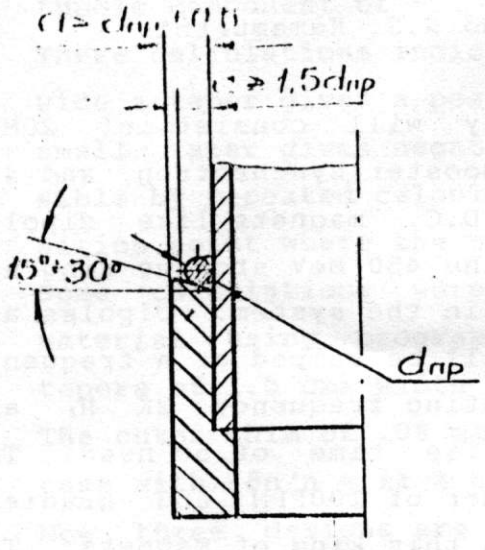

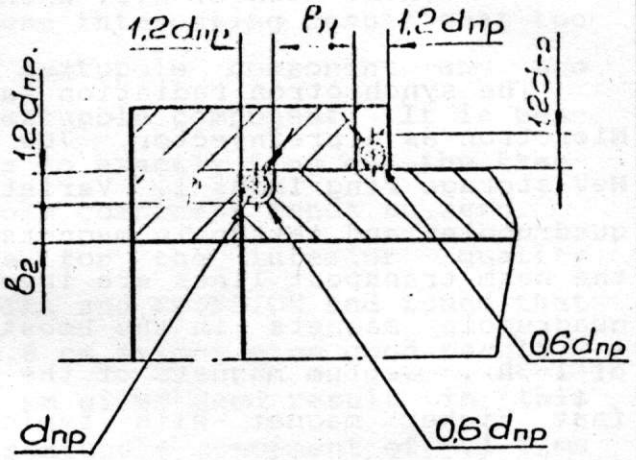

$B_1 + B_2$	6	12	20
$d_{пр}$	1	1.6	2

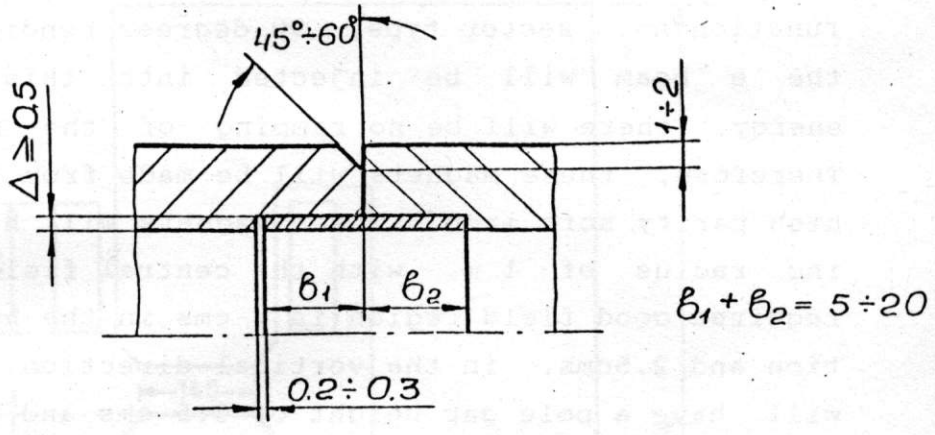

Fig. 8

EVOLUTION AND STATUS OF THE CONTROL SYSTEMS OF THE ACCELERATORS AT THE INP

E.A.Kuper, G.S.Piskunov

Institute of Nuclear Physics, 630090 Novosibirsk, USSR

Abstract

The historic review and current state of the accelerator control systems at the INP is presented. Questions concerning organization of distributed multiprocessor systems as well as specific features of measuremnt and control devices are discussed. The structure of the control system for the VEPP-3 storage ring, based on the use of CAMAC-oriented 24-bit microcomputers is described.

History and Principles

First experiments on the application of computers for accelerator control began at the INP in 1970 at the storage ring VEPP-3 when the necessity arose to increase the luminosity of the storage ring by changing the magnetic system of the experimental straight section in the presence of a circulating beam, the latter requiring high precision and matching of a change in the characteristics of the magnetic structure components. For this purpose, a second generation computer "Minsk-22" was employed, whose control program was written in machine codes. Since 1972 a deal of effort has been undertaken in the automation of both the existing accelerator facilities and those being under construction: VEPP-2M, NAP-M (in the 1970s), VEPP-4 (1978), SIBERIA-1, BEP (in the 1980s) and some others.

In the first systems only the most vital parts were automated, i.e the power supply for the magnets. Later the computer control covered a greater and greater number of the subsystems with the ever-decreasing share of manual control. So, the VEPP-4 facility was designed from the beginning to be completely computer-controlled. The use of duplicate manual control subsystems at the facilities of such a scale proves to be very expensive. This lack of the possibility of manual intervention in machine operation gives rise to a specific requirement for control equipment: the last commanded settings must retain in it irrespective of the computer availability. This absence of duplicate manual subsystems is characteristic of the up-date INP control systems.

When designing the very early versions of the VEPP-3 control system the decision has been made not to engage professional programmers. In fact, since they are not experts in the questions concerning the operation of particular subsystems of the facility, they are unable to write programs with due regard of the specific nature of a task. At the same time, the complexity and experimental mode of the operation lead to hardly identifiable, diffuse specifications in the definition of a problem. In these conditions, it seems more effective to engage in the development of applied software the persons who possess a practical knowledge of the facility operation.

At present the control systems of the main acceleration facilities of the INP comprise microcomputers compatible with the Odra-1300 series. The choice of "Odra-1304" for the VEPP-3 control system in 1972 was largely a matter of chance. However, the use of this machine has had a pronounced effect on further development of control systems at the INP.

Computers of the Odra-1300 series are functionally analogue to the known family ICL-1900, designed in the late 1960s. They are classified as universal computers and had much better parameters compared to minicomputers which have been in common use in the 70s. The application of a sufficiently powerful computer to the control system has enabled one to reach a high level, qualitatively different from that provided by the minicomputers available. A considerable, at that time, memory size as well as high throughput offered the possibility of creating the neccessary software for control systems, exclusively in high level languages and, consequently, has made it possible to involve, in the software development the machine staff.

The open nature of the most dynamic component of control systems, the software and the possibility of its extension and modification by the machine staff are typical for most of the INP control systems. Consequently, one of the principles which we tried to follow was: applied software should be designed by the persons who are expected to use it. To do this, it is very desirable to ensure the possibility to use a high level language in the environment of a friendly system for program preparation.

Structure of the hardware and the choice of a computer.

In solving the problem of efficient communication between computer and control hardware we came through several stages. At first stage, i.e. when putting the VEPP-4 control system into operation, the most of the control hardware was made using mechanical standard for nuclear electronics called "Wishnya" as the so-called autonomous functional units (AFU). The AFU were designed for the solution of particular tasks on the basis of standartized PC boards: memory, state machine, interface with data transfer network, multichannel ADC or DAC.

Simultaneously with the accelerator cycle, the AFU performed the measurements and stored measured values in the internal memory. The interaction with a computer was limited to writting or reading the blocks of structured data from that buffer memory. The computer operating system (OS) overhead to initiate the transfer of a large block of information through the DMA channel of the computer had little effect on the total throughput. All the devices were connected to the computer through a serial data transmission network having a three-level tree-like topology.

The VEPP-4 control system was designed on the basis of such a scheme. It included 6 computers "Odra-1325": one machine for each of the subsystems such as an injector, an intermediate storage ring VEPP-3, main ring VEPP-4, and a high frequency generator "Gyrocon". Later one more computer for supervision of the technological parameters of the entire facility (vacuum, temperature, radiation, etc.) was added. This system operated in 1978-84.

The life time of an accelerator lasts usually several decades. It is modified all the time because new ideas and new demands appear. The control system must evolve in time together with the accelerator. Continuous modernization of the control devices on a long range perspective has necessitated the changeover to a more universal, computer independent standard. At this time the only suitable was CAMAC. A transition to the CAMAC standard was also stimulated by the need in the unified hardware in the frames of the whole Institute. Since 1978, almost all the electronic equipment intendend to be used in the control systems was implemented in CAMAC.

System integration in the CAMAC standard has some bottlenecks, due to a high intensity of interaction with the computer, which is inherent to the standard. In essence, CAMAC is intended for the use of the so-called program I/O. In our case, Odra-1325 computers did not even posses instructions on the user level to perform the I/O - all had to go through the multitasking OS, which led to a very high overhead. This is a typical problem for modern minicomputers with complex multitasking OS.

The first step in the solution of this problem was a development of a dedicated crate controller connected to the serial data transfer system and performing the simplest interactions with the modules in the crate. In the controller there was a memory containing the previously written control information: N, A, F, waiting of Q, LAM, a branch to the next instruction, etc. Such a controller makes it possible to perform the required low level control actions and transmit to a computer only the "pure" structured data. Although this controller has enabled to achieve satisfactory time characteristics; however, in the multiprogram environment inherent to the control systems, the problem has arisen of an arrangement of the controller-to-programs interaction, because several programs had to share the same control memory of the controller.

The next step was the use of an intelligent crate controller being a 16-bit microcomputer with a simplified instruction set and a small memory. Its application encountered the known problems typical for many systems at the late 70s: a minicomputer, at the top level, and an intelligent controller based on a low-power microprocessor, at the lower one. The major disadvantage of these systems is the complexity of controller programming to be done in assebler by experienced programmers, and this violates the principle stated above: the software is designed by the physicists. For this reason, such controllers have found its application only in the fixed task systems, where no modification of the programms was needed.

A radical decision was made in the late 1981- to design an intellectual crate controller with the instruction set of Odra-1300 computer. This allowed us to modernize hardware and to retain most of the software. In 1983, such a controller, "Odrette", was ready for operation. It was first used as a slave processor in the Odra-based systems. In the summer of 1985 we abandoned the further use of the Odra computers and began to employ only the Odrettes.

Odrette occupies doublewidth module in the controller position of CAMAC crate. In fact, it is a 24-bit computer with Odra-1300 (ICL-1900) instruction set. Its basic features are:

- address space 4M words;
- on-board memory 64K 24-bit words;

- performance - 0.4 MIPS;
- hardware implementation of floating point operations;
- User / System modes;
- multitasking support / memory management unit;
- CAMAC oriented I/O instructions;
- vector and vector/scalar operations;
- bit-slice implementation based on AMD 2900.

The bit-slice implementation has offered the possibility to change the original architecture in the desired direction. Besides the introduction into architecture instructions to interact with the CAMAC bus, some important modifications, useful in real-time systems, have been done. Among such innovations was the mechanism of process switching. The point is that the availability of the multitasking is of principal value for a computer used in control systems. The systems designed to control the accelerator, in which the accelerator is not only a tool but also an object of research, are characterized by frequent changes in the regimes and configuration, by presence of a great number of research problems. Multitasking allows easy split of a complex control task into a number of smaller ones, while interaction between tasks is organized by the OS. Operating system regards all the tasks waiting for LAM signal or program "event" as being active. On occuring the expected event, the processor initiate, at the microprogram level, the needed program according to its priority. Thus, the most time critical part of the multitasking OS was implemented on the microprogram level. This led to more than an order of magnitude improvement in the time response.

CAMAC modules for the control systems.

One of the peculiarities of our laboratory is that almost all the electronic equipment intended for control systems is developed and assembled in the Institute. The ever-increasing complexity of the accelerators and the experiments which they involved in often specify the requirements for the parameters and the structure of the modules being designed. The metrological characteristics, throughput and noise immunity must be adequate to the operating conditions of the system.

For example, when solving the problems of the transportation of reference voltages in the power stabilization systems, digital-to-analogue converters based on a principle of pulse width modulation (PWM) are in common use. An 8-channel CAMAC module placed in the crate, generates width modulated signals, transferred over galvanically isolated coaxial cable directly to the point, where the reference voltage is needed. There the PWM signal is converted into analogue form. Thus at minimal expenditure an accuracy equal to 0.01% is achieved. For high precision systems a PWM-DAC with an accuracy 0.001% has been developed.

The control systems are also responsible for numerous multichannel measurements of DC and quasi DC voltages. In this case, the sources of signals are often far from each other. To achieve the necessary interference suppression, integrating ADCs have been designed with variable integration time of the input signal. Depending on the required precision, the measuring time is program-ranged from 5 to 320 ms, the scale varying from 13 to 20 bits. The ADC accuracy is 0.01% in the 20-50 C temperature range. It has floating analogue part. To

arrange multichannel measuruments, the ADCs are equipped with 64-channel two-terminal analogue multiplexers.

The necessity to analyse the shape of pulse signals has given rise to the new class of devices - transient recorders. These devices comprise a fast ADC, control circuits, internal memory and an interface allowing an on-line control of discretization frequency and a change of the input voltages range. The detection and analysis of the shape of pulsed signals in different systems by the ADC with further computer processing have enabled a number of important problems to solve:

- monitoring the behaviour (current and coordinates) of the beam during the first several thousands turns of injection;
- observation of small amplitude signals in presence of a heavy but repetitive enteference by means of a preliminary digitazation of the interfering signals in the absence of an useful one with subsequent substraction from the sum signal;
- detection and studying the evolution of the non-predictable events by writing the measured results in a ring buffer, with a stop when an event (say, a beam loss) appears;
- as a program controlled oscilloscope.

We present here the main parameters of the two most popular recorders. For the ADC101S, they are: 10 bit resolution, minimal sampling rate 1 us, memory capacity 4 K words, 400 kHz bandwidth. For the ADC850S they are: 8 bits, 50 ns, 1 K words and 4 MHz, respectively.

Besides the devices mentioned above, a great variety of modules necessary to ensure the functional completeness of the set have been designed. The total number of different types of modules developed exeeds 100. There are the generators of time intervals, timers, meters of instantaneous values of the pulse signals, multichannel modules required to monitor such mass parameters as vacuum and temperature, position transducers, output registers, colour graphic displays, etc.

Software of the control systems

The software of the early INP control systems (VEPP-3, 1973-77; VEPP-2M, 1974; NAP-M, 1975) was based on the use of interpreters. The interpreter of the VEPP-3 control system on an Odra-type computer was a complex overlay program, written in FORTRAN, which implemented, besides the functions of executive system, the function of a text editor of the source programms-"processes", a librarian, a magnetic tape backup server and many others. The programming language, specified by this interpreter, has offered the possibility of arranging, despite an awkward syntax, rather complicated algorithms in control processes. Many ideas on the arrangement of the control process have still remained useful and have found its implementation in modern control systems of the INP.

It seems rather simple to implement the programming language of the control system on the basis of an interpreter. This approach inevitably limits the possibilities of evolving the system: the access to the control system gets limited by the frames of a single exotic language, and the latter, because of its specialized nature, may prove to be inadequate to new problems. In addition, interpretation considerably slows down the execution of the programs.

With this in view, when designing the VEPP-4 control system, an interpreter has been dropped and the designers have

aimed on developing a multitasking operating system. In this case, the system is not referred to any language and both the interpreting and compiling programming systems may be used. All the programs, used in the control system, are written in a FORTRAN-like language TRAN whose compiler is an integral part of the program preparation system.

The program preparation system comprises a screen text editor, a compilation system, a library maintenance program and some utility programs.

The compilation system consists of various translators, consolidator and loader. All the used translators generate ICL-standard intermediate code and then a consolidator unites them in a single program. At this stage the fragments written in different languages may be consolidated in one program. The major language in the system is the TRAN mentioned above, which is an extended subset of FORTRAN. The entire compilation system is rather fast and it takes about 30 seconds to translate, link and load into memory a program of average size (1.5-2 thousands of lines).

The system of program preparation relies on a large library of subroutines, which offers to a programmer a wide choice of mathematical functions and also a set of procedures intended for interaction with devices of the control system, terminals, graphic displays and files, as well as interaction with the OS and other programs.

The OS of the VEPP-3 and VEPP-4 control system offers a standard enough set of functions of modern real-time operating system: memory managment, processor sharing, arrangement of the access to the standard peripheral devices, file management, synchronization of the control programs operation via the system of external interrupts, interprogram message passing, etc.

The content of the applied software for the VEPP-4 control system may be illustrated by a set of programs running in the main computer of the facility in the stationary regime:

- BANK program working synchronously with a peripheral timer and by means of which all the remaining programs get acces to the equipment of the control system;
- a program-process providing the particle accumulation, a raise of the beam energy up to the energy of the experiment with the ordered parameters of the beams;
- a program of "manual" work, which permits one to change the operational mode of any component of the storage ring;
- a program intended to measure the beam luminosity and polarization;
- a program holding the position of the collision point with respect to the angle and coordinates.

Besides the above programs, a watchdog program is resumed in each 5 minutes which checks the agreement between the state of the storage ring components with the values held in the machine's data base. In addition, the operator can initiate the programs which measure the parameters he is interested at the moment, and which are not subject to regular supervision.

The control systems mentioned above are distinguished by the use of a single control computer. With the appearance in the system of an "intellect" allocated in several lower-level microcomputers, some difficulties in the arrangement of their effective use have been revealed. In similar multiprocessor structures, it seems difficult to split the functions of the control programs into the pithy fragments suited for separati-

on in some of the processors because of the strong information links between the subsystems of the facility. For this reason, Odrettes were initially used as auxiliary low-level processors responsible for the solution of isolated enough problems.

As the experience in the use of Odrette has been accumulated, it has become evident that such a structure of the control system interfers with its further evolution and that the switchover to the distributed structures is inevitable. At the same time, the creation of a distributed system specifies new requirements for the system software and lead to a certain redistribution of the responsibility for the support of the system functions. So, for example, the programs in different processors should be linked in a unified way, at the level of operating systems, which also arrange a joint access to the common data bases and provides the sinchronization of the processes throughout the network.

The distributed systems may be arranged in a certain hierarchical order. However, the functions of a central computer reduce, in a definite way, to the functions of a file machine which offers the peripheral computers the resources such as disc space, terminals, printers, as well as possibility of access to the archives on magnetic tapes. In this case, the choice of a topology for the network has a lesser influence on the architecture of the system as a whole. So, we have chosen a star like configuration since it is the simplest in implementation, though the ring and bus structures are possible as well.

The new function, not implemented in the early operating systems is the provision of an interprogram interaction for the programs running in different lower-level processors. In this case, it is desirable to ensure a maximum unification of the program interfaces of a peripheral operating systems for the exchanges of various types: interprogram in the same processor, interprogram for different processors, program exchanges with both the files placed on a disc of a given computer (local files) and the files placed on the discs of a file server.

The current status and the aims

At the present time, the control systems of two big accelerator-storage facilities of the INP, VEPP-2M and VEPP-4, are being updated and, in particular, the switchover is made to a distributed control system on the basis of a microcomputer Odrette.

The shutdown of the VEPP-4 facility for modernization has enabled us to avoid a gradual transition to the distributed control system and to make it at once, without the stage of coexistence of the old and new systems. At present, the new control system covers injection part of the facility, that comprises a linear accelerator with Gyrocon-based RF system, a synchrotron B-4, beam transfer lines, and an intermediate storage ring VEPP-3. For control, this part of the facility is divided into two, weakly linked subsystems: control of the injector and control of the storage ring.

Now the functions of the computers, forming a star structure, are assigned as follows:

- The central top level computer with 56 Mb winchester disk serves as a file and network server for peripheral processors. There is also a link to Odra-1305 computer

(George-3 operating system) providing file archive servises with automatic magnetic tape backup. In total there are 16 Odrettes in the system connected the central one via a serial 3 Mbit/s links. Apart from providing the file servises, the central computer is also responsible for message passing between tasks in different processors of the network, virtual terminals support, mailboxes, etc. The message passing and file exchange mechanisms are implemented in an unified way.

Eeach peripheral subsystem based around one Odrette may reside in a single or in several CAMAC crates. Additional crates are connected to the one containing processor via a serial 10 Mbit/s driver and a simple non-intelligent controller. The time requied to transmitt 24 bits of data on the CAMAC bus in local crate (containing the CPU) is about 25 us. In the block transfer mode the rate is 300,000 24-bit transactions/s.

The operating system of the peripheral Odrette provides support of up to 4 local terminals (connected to the local crate) and additionally up to 4 virtual (network) terminals. There may be up to 10 memory-resident independent tasks, scheduled on a simple priority basis or on the round-robin basis for the tasks with equal priority.

The Linac is controlled by three microcomputers with the functions assigned as follows: control, monitoring and supervision, beam parameters measurements.

The control equipment is placed in 12 CAMAC crates. At present, there are 260 measurement channels and 230 control ones, and the control channels will be further increased in number.

The applied software of the injector subsystems comprises 5 continuously running programs and some set of auxiliary ones whose execution is initiated, if necessary, by operator or by one of the running programs. An interaction between the control and monitoring equipment is performed by means of two BANK programs working, correspondly, in the control and monitoring microcomputers. The rest of the programs recieve the needed information from them over the interprogram links.

The information, necessary for an operator, is output to a CRT terminals or graphic displays. An operator-machine dialogue is carried out mostly via a terminal.

The injector data base consists of two parts: the first includes a description of the elements (address, access rights, scaling factors, etc) and the second contains the table of regimes.

The storage ring VEPP-3 is also controlled by three microcomputers with the following assigned functions:

- control and monitoring of the magnetic system of the storage ring;
- control and monitoring of the RF system;
- measurement of the beam parameters (currens, closed orbit, betatron oscillations frequency, etc.).

The equipment is distributed over 10 CAMAC crates; the number of the control points is 200 and that of monitoring is 500.

Now the applied software includes 8 main programs. The principle of interaction of the programs with the control and monitoring devices is the same as in the injector subsystem. To set the regimes, there exists a program enabling one to change "manually" settings of the elements within a given

regime. The program also accomplishes a comparison of the given regime with the current state of the storage ring components.

The general volume of the applied software for the injector subsystem is about 20000 TRAN operators. And its volume grows rapidly as the system evolves.

Since we are not quite experienced in the use of the distributed control systems, we are planning to perform, in the nearest future, a comprehensive analysis of the possibilities and operating characteristics of the systems described above to reveal possible bottlenecks and to outline the ways of their further improvement and development.

DIFFRACTION EXPERIMENT AT SIBERIAN SR CENTRE

B.P.Tolochko[1] and M.A.Sheromov[2]

[1]Institute of Solid States Chemistry, 630091 Novosibirsk, USSR
[2]Institute of Nuclear Physics, 630090 Novosibirsk, USSR

A crystallographic synchrotron radiation station installed at VEPP-3 is mainly intended for experiments aimed at, first stage, is speedy high-resolution data collection from macromolecular crystals with large lattice periods. Later on, with improvement of facilities and techniques the unique possibilities of the synchrotron radiation will be extended to the solution of more complicated problems of macromolecular crystallography.

With regard to this aim, the optical system of the station should provide:

1) beam focusing on a detector to a spot 0.5-0.5 mm^2 in size;
2) possibility to work with a given wavelength in a wide range of wavelengths from 0.6 to 1.8 Å:
3) beam monochromatization with $\delta\lambda/\lambda \sim 10^{-3}$.

The instrumental set-up of the station is given in Fig.1. The station is positioned in the synchrotron channel 5 of the VEPP-3 wiggler. In front of the crystallographic station in the same channel there is an X-ray microscopy station which can be removed from the beam when the crystallographic station is in action. Beam monochromatization is ensured by a perfect triangular single crystal which can be curved to provide for focusing in horizontal plane. The distance between the source and the monochromator is 17 meters. Automatic horizontal and vertical slits are placed 5 meters ahead the monochromator in a vacuum protection box to cut the white synchrotron beam on the monochromator. In this box there is also a two-crystal monochromator of the microscopic station which is removed from the beam when the crystallographic station is at work. In future we intend to use this monochromator together with the focusing one-crystal monochromator to obtain high energy resolution in anomalous scattering experiments.

A one-crystal monochromator is mounted on the lower flange of the cubic vacuum box. The white beam is injected from two counterfacing side entries and the monochromated beam exits from the opposite side, while the wall flange parallel to the

synchrotron beam has an observation window. The other holes are covered by blind flanges. The box is made of stainless steel, its walls are 20 mm thick, providing for radiation safety of the personnel. The synchrotron beam enters the monochromator box travelling in a vacuum telescopic tube which is shortened during the operation of the X-ray microscopic station. Inside the box besides the monochromator there is a block of automatic slits to reduce background radiation.

An Arndt-Wonacott photocamera (ENRAF-NONIUS) is used to collect X-ray data from single crystals. The usual distance between the monochromator and the sample is 4.3 m and can be changed, if necessary, within the range 2-4.8 m. A monochromatic beam falls onto the sample from a vacuum telescopic tube coming from the monochromator box. Between the tube end and the photocamera collimator there are manually set vertical and horizontal slits, ionization chamber, background screen to protect the film from background effects. All these units, together with a photocamera, are placed in a hutch which provides radiation safety of the station personnel during operation. The hutch and the telescopic tube are mounted on a bench 5 meters long which rotates about the vertical axis of a co-axial axis of the monochromator when the wavelength is changed. The angle between the primary and the monochromated beam can be varied from 15° to 32°. This range is limited by the location of the neighbouring stations.

In the near future the station is due to be equipped with an automatic focusing segmented mirror and an automatic tuning carriage for the photocamera. The mirror will be placed behind the focusing monochromator which should eliminate radiational and thermal instability due to the mirror action in a direct SR beam. The mirror will comprise eight planar segments made of polished glass measuring 200 x 50 x 25 mm^3 each. The segments will be positioned to form a surface imitating an elliptical cylinder. The segment motion will be ensured by eight stepping motors computer controlled via CAMAC blocks. The segment movements will be registered by absolute position counters on the basis of multirotational potentiometers. Up and down shifts of the whole mirror unit as well as its inclination will be provided. The mirror and the motors will be in a vacuum. The mirror should provide beam focusing in a vertical plane and eliminate the high harmonics of the beam reflected

from the monochromator. The latter is of major importance in view of the work with superconducting wiggler with λ_c = 1 Å which is planned for the beginning of 1989.

The automatic tuning carriage will provide tuning of the photocamera in radiationally secure conditions. It will shift the photocamera in the horizontal and vertical directions and turn it about the vertical and horizontal crossing axes.

Triangular shaped monochromator crystals prepared from perfect Ge and Si crystals are widely used in different synchrotron stations. Such monochromators provide a fairly high beam monochromatization ($\delta\lambda/\lambda \sim 10^{-3}$) and enable one to focus almost the whole synchrotron beam on the sample in the horizontal plane. Beam focusing is achieved by curving the crystal as a round cylinder on pressing the triangle tip and compressing the base. Reflection from (111) crystal plane is most commonly used; the crystals are cut so that the reflecting plane makes an angle α with the crystal surface. An oblique cut makes it possible to compress the diffracted beam A times, where $A = \sin(\theta+\alpha)/(\theta-\alpha)$, where the intensity of the reflected beam is $A^{1/2}$ times lower, beam density being $A^{1/2}$ times higher than that in symmetrically cut crystal. As the white beam falls onto the monochromator the latter functions as a mirror. If the radius of curvature R

$$\frac{2}{R} = \frac{\sin(\theta+\alpha)}{p} + \frac{\sin(\theta-\alpha)}{p'}$$

where P and P' are the distances between the source and the monochromator and between the monochromator and the focusing point, respectively. The lowest $\delta\lambda/\lambda$ is achieved if the focusing is made at a distance P' = P/A (Guinier condition). In a general case

$$\frac{\delta\lambda}{\lambda} = \left[\left(\frac{b_h}{p} + \frac{L}{2}\left|\frac{\sin(\theta-\alpha)}{p'} - \frac{\sin(\theta+\alpha)}{p}\right|\right)^2 + \omega_{sym}/A\right]^{1/2} \cot\theta$$

Taking into account system aberration, the resulting focus size is:

$$f = \left[\left(\frac{b_h}{A}\right)^2 + \left(p'\omega_{sym}\right)^2 A + \left(rL^2/8R^2\right)^2\right]^{1/2}$$

where $r = R\cos(\theta-\alpha)$

r is the radius of curvature of caustic surface of the focus, ω_{sym} is the width of the rocking curve of the monochromator crystal, L is the length of the monochromator crystal. Knowing the value of flux density spectral distribution we can evaluate the flux density at the focus

$$\rho_{mon}\left[\frac{photon}{s\cdot\mu rad\,\mu A}\right] = \left(\rho_{source} I\right)\frac{L\sin(\theta+\alpha)}{p}\cdot$$

$$\frac{1}{(p+p')\Psi_v}\cdot\frac{1}{f}\cdot\frac{\omega_{sym}\cot\theta}{A^{1/2}}\cos 2\theta$$

where ρ_{source} is the flux density at the source $\frac{photon}{sec\cdot\mu rad\,\mu A}$ vertically integrated with $\delta\lambda/\lambda = 1$.
Here I - electron current, cos 2θ - polarization factor.

Si crystal 120 mm long cut as a triangular plate is used as a monochromator, the plate surface making an angle α = = 8.25° with the (111) plane. The monochromator design resembles an automatic goniometer head. The main rotation about the vertical Ω axis for tuning to the needed wavelength can be performed with a "rough" step $\Delta\Omega$ = 1.3' within the range of angles 60° and with a fine step $\Delta\omega$ = 0.4'' within the range 3'. When the monochromator crystal is curved its edge is shifted with steps 1.5 μm. The adjustment can be made by rotation about two perpendicular horizontal axes with a step 0.3', as well as by shifts in the directions vertical and perpendicular to the beam with a step 5 μm. The motion is provided by stepping motors; the monochromator position and the motors operation are controlled by multichannel potentiometers. The monochromator is computer controlled via standard CAMAC blocks.

The estimation of calculated characteristics of the monochromated beam λ = 1.38 Å (absorption edge for Cu) and P' = = 4300 mm gave the value of f = 750 μm and ρ_{mon} = $1.5\cdot10^{10}$ photon/s·mm^2.

The flux density estimates were carried out using ionization chamber, placed behind the collimator of the Arndt-Wonacott photocamera; collimators with diaphragms 0.6, 0.4 and 0.3 mm in diameter were used. Beam width estimates were made by shifting a small vertical slit with a step of 50 μm. The slit was facing the ionization chamber. Judging by the flux density

estimates one should expect the data collection procedure to become 20 times faster than that in experiments with a rotating anode tube equipped with focusing optics ($\rho_{tube} = 9 \cdot 10^8$ photon/s·mm^2). The use of superconducting wiggler source, installation of a focusing mirror and the use of a larger Ge monochromator crystal (instead of Si) will increase the flux density by a factor of 20÷30.

Monochromator tuning to a given wavelength and to the maximum intensity is carried out using an ionization chamber and a set of foils with known absorption edges. To estimate beam stability and control data collection we use an alphabetic display and a graphic display. The standard Arndt-Wonacott camera was modified to decrease the error due to a gradual decay of the beam intensity with time (on the average, the synchrotron beam of the VEPP-3 storage ring loses 1% of its intensity every 3 min). This modification allowed data collection at fast rotation rates when the number of oscillations was large. Thus, the error due to beam drift was lowered to a certain allowed level.

Several check-up experiments were carried out on this station and we could therefore make a plan for the future work. Arrays of crystallographic data were collected for catalase from Micrococcus lysodeikticus at a resolution of 1.8 Å, and for pyrophosphatase from E.Coli at a resolution of 2.45 Å. In both cases a fairly high resolution was attained, in contrast to the use of conventional X-ray sources for data collection from protein crystals with relatively large unit cells. Catalase measurements lasted 10 hours, pyrophosphatase measurements - 6 hours. In both cases only one sample of each protein crystal was used, which is especially important for pyrophosphatase; its effective lifetime increased at least by a factor of 6. Catalase crystals are more durable.

The time-resolved diffraction station operates in sequence with the crystallography station and comprises the same optic elements: a focusing monochromator, slits; in the forthcoming experiments a focusing mirror is expected to be used. The basic component of the station is a vertical goniometer of the PW-1050/81 type, manufactured by Philips (Netherland), with a one-coordinate detector installed at it. The goniometer is positioned on an adjustment table (see Fig. 2). By means of vertical displacements and rotations about the vertical axis, the

goniometer is placed parallel to the SR beam such that the beam passes through the centre of the instrument.

The coordinate sensitive detector developed at the INP, Novosibirsk, is used at the station. The detector is a proportional chamber whose cathode performs as a delay line. Such a scheme enables one to detect the coordinate of an incident quantum by the time difference between the pulses from different ends of the delay line. The detector resolution is 0.1 mm. The input window length is 100 mm. The maximum counting rate is 250 kHz.

Fast time-to-digital converter (TDC) is used to determine the coordinate of a quantum reaching the detector. The TDC resolution is 400 picoseconds, its maximum counting rate is 500 kHz. The quantum coordinate is recorded in the memory device (MD) in the form of numerical code. In order to increase the rate of the data transfer from TDC to MD, the operation mode through the front panel is used. Recording is performed in the increment regime. The single MD capacity enables one to store up to 64 X-ray diagrams registered by the detector. Each X-ray diagram has its own individual zone in the MD - a "page". The change of the zone address for recording new X-ray diagrams is performed by a special program recorded in the crate-controller. In such a mode one can "turn pages" in one millisecond, with an interval of 10 microseconds between pages. As a rule, 64 X-ray pictures recorded in one MD are not enough for the whole picture of the dynamics of the process under study. Therefore, the possibility of operation with a number of MDs (up to ten) is envisaged. In this case, all MDs are connected in parallel with the TDC through the front panel.

The automation system developed at the Novosibirsk INP on the basis of the computer ODRA-1325 is used to pick up information stored in terminal devices, and also for the operational control of the whole station. This system comprises both the hardware and the software of the computer-station communication.

To study the structural changes occurring in single crystals it is most optimal to use detectors on the basis of CCDs (charge-coupled device-detector). A CCD-detector has a number of advantages over a one-coordinate detector operating in the proportional regime. First, a CCD has no restrictions on the counting rate, whilst a proportional detector has a maximum counting rate of 250 kHz. This is due to the fact that an in-

crease of the diffracted radiation flux leads to increasing the charge collected in the CCD cells as it is emitted by photons. Second, a CCD-detector possesses a better spatial resolution - 15 μm. Third, for a CCD, the time needed to record a radiograph can be, in principle, decreased down to a few nanoseconds. Unfortunately, this device has a small cell for detecting (10 x 10 μm), low efficiency (5% for the radiation from a copper X-ray tube), whereas the time to read out the information arrived from the detector and to transmit it to the computer memory is large (300 ms).

To automate the works involving diffractometers with the use of SR from VEPP-3 and to make a preliminary processing of the information obtained, the computers ODRA-1305 and ODRA-1325 have been in use. For the performance of a diffractometer to be directly controlled, the following moduluses manufactured in the CAMAC standard were used:

-UShD-2 - an unit to control stepping motors; it is used also to rotate the monochromator, detector and a sample on the goniometer and for the other purposes;
- P-2 - a hand-operated unit to control stepping motors;
- KAS-32G - a 32-channel commutator;
- SG-2 - a stepping motor digital;
- TsDR-2 - an unit to control a color display;
- ATsP-101 - an analog-to-digital converter;
- TsAP-16x16 - a digit-to-analog converter.

During the adjustment and tuning of the diffractometer to the required wavelength the performance of its basic units is controlled by means of a terminal. For convenience, all information on the performance of the units is displayed on a color display. If necessary, an operator can stop the program and to make the required corrections. For recording the experimental data as soon as a computer instruction arrives, the recording system starts to work.

The small-angle scattering station is positioned at SR channel 5 in the VEPP-3 bunker and works in sequence with the crystallography and time-resolved diffraction stations. Until now A.A.Vazina's team (Institute of Biophysics, USSR Academy of Sciences, Moscow) who developed the station has used a rectangular focusing monochromator with a four-cylinder crystal bender and a one-section focusing mirror. In the nearest future, a focusing monochromator with a triangular crystal and

a multisectional focusing mirror will be in use. The station is involved in the examination of bilogical objects the diffraction picture of which is concentrated within 1'÷2-3°; note that in this range there are tens of diffraction maxima and the angular distance between them is a few mrad.

To improve the angular resolution, a one-coordinate detector is placed a few meters apart from a sample. A long path of the X-ray beam in the air leads to a considerable degradation of the intensity because of the absorption and the appearance of parasitic radiation at X-ray beam scattering. To avoid this, the path of the X-ray beam must be exhausted.

The detection system is made in the CAMAC standard. Elektronika-60 is employed as a control computer for the station. The time resolution achieved at the station is 10^{-3} s. This allows one to study the dynamics of structural changes of fast processes, in particular the dynamics of muscle contraction. A 3-dimensional hystogram of the time dependence of the scattering curve after *A.A Vazina* is given in Fig. *11*.

The anomalous-scattering station is intended to overcome some difficulties associated with the "phase problem" in crystal structure determination. When analysing the structure of a substance consisting of the same atoms, the question on a possible change of the phase upon scattering on the crystalline lattice has no practical value. This change can have influence on the phase of the resulting scattered wave, rather than its intensity. However, the situation changes if the unit cell comprises more than one kind of atoms. For different atoms, the change in the phase after scattering can be different from those determined by the atomic position in the unit cell. Such variations in phases may be taken into account if we assume that the atomic scattering factor f is of the complex form:

$$f = f_o + f' + f''$$

where f' and f'' are real and imaginary parts of the "anomalous" scattering since the complex amplitude always incorporates the phase factor. Then,

$$f = f_o + \Delta \cdot e^{i\varphi}$$

where

$$\Delta = \left[(f')^2 + (f'')^2 \right]^{1/2}$$

$$tg\,\varphi = f''/f'$$

determine, correspondingly, the real amplitude factor equal to the modulus Δ and the phase factor $\varphi = arctg(f''/f')$. They account for the absorption of the X-rays by the electrons of finite binding energy in the atom. The f' term represents in-phase scattering and the f'' term represents scattering shifted by 90° in phase. As for many types of dispersion phenomena, f' and f'' are linked by a Kramers-Kronig relationship. Close to the absorption edge ($\pm$100 eV), f' and f'' vary rapidly with wavelength. There is a sharp jump in f'' from below toabove the edge (in energy) while f' dips to a large negative value through the edge.

As is well known, obtaining the diffracted intensities from a crystal is not the only step in the crystal structure determination. The "phase problem" must also be solved. The diffraction pattern of a crystal is the Fourier transform of the electron density within the unit cell. The transform has an amplitude and a phase component, but only the amplitude can be directly measured. Normally, the phase is obtained by preparing a second crystal that is identical to the first except for the inclusion of an extra atom, preferably a heavy one, such as platinum or mercury. This is known as the isomorphic derivative of the native crystal. Comparison of the two diffraction patterns gives the needed phase information. Actually, several derivatives are usually necessary.

The same information can, however, be obtained by varying the photon energy of the X-ray beam. For each element, there are characteristic photon energies (absorption edges), below which there is an energy insufficient to excite electrons out of an atomic shell, but it is above the edge. Thus, by simply tuning the beam across the absorption edge of the heavy atom, the effect similar to making an isomorphous derivative can be obtained. Above the edge, the atom absorbs and appears not to be in the structure and below it scatters X-rays into the diffraction pattern instead of absorbing and is thus "in" the structure. This phenomenon is called "the anomalous scattering".

For the characteristic radiation from X-ray tubes, the anomalous additions to the atomic scattering factor have been calculated theoretically. These data are generally accepted now and are broadly used by specialists in crystallography to identify the structures. It is beyond doubt that the theory of anomalous additions is valid and may be applied for all wavelengths. However, in close vicinity to the absorption edges this theory does not work because it omits the effects occurring at resonance excitation of the orbit electrons. A lot of experimental works are devoted to the studies namely in this narrow range of wavelengths.

The anomalous scattering station is positioned on SR channel 2 of the VEPP-3 wiggler and is 10 m distant from the radiation point. At a distance of 6.7 m and 9 m from this point, there are a vacuum seal and slow and fast shutters, respectively.

A monochromator is placed in an exhausted steel box. The insertion of the monochromator into the vacuum chamber is aimed at the following: 1) to eliminate the beam attenuation in the long-wave spectral range, 2) to prevent the formation of oxide films on the surface of a crystal and also the corrosion of some units of the monochromator, which takes place when SR is used in the atmosphere, 3) to reduce the radiation background because of the fact that SR is scattered in the air, in the monochromator chamber. The crystal-monochromator is fixed on a precision goniometer installed at a vertical stage. Crystal rotation and translation in the vertical direction are driven by stepping motors. The scanning step of the monochromator is 0.38'' and that of the vertical translation is 0.1 mm. Each step of a motor is monitored by an optic digital counter. Since the rocking curve of the crystal Si(220) reflection yields the intrinsic energy resolution $\Delta E/E = 5.6 \cdot 10^{-5}$, the energy resolution of the experiment is $\sim$ 1.0 eV for 11 keV photons. In anomalous experiments, also used are Si and Ge perfect crystals cut with its (111) crystal plane at an angle α to the crystal surface. The required wavelength was selected automatically by a special routine. For this purpose, each discrete position of the monochromator is previously calibrated at the wavelength corresponding to the K-edges of the elements introduced into the SR beam. The elements were chosen such that their K-edges were within the working region of the experiment.

After the scanning over the whole range of wavelengths the diffraction angle and the corresponding wavelength along which the maximum absorption at the K-edge of an element was observed were fixed in a computer. The wavelengths corresponding to the angles of the monochromator were calculated by computer and written in a calibration table.

Two Ta slits, necessary for collimating the primary and monochromatized radiation were also placed on the same vertical stage. Both slits are adjustable for height independently, but this procedure is made very rarely, because the monochromator is aligned by displacing three elements (two slits and a goniometer), which are strongly linked with each other. The monochromator is aligned by a computer routine which determines a maximum of the monitor intensities. Behind the monochromator there are a monitor and a collimator. Primarily, we used an ionization chamber as the monitor; however, our experience have shown that if the diffracted radiation is detected by a scintillator-detector it is more efficient to use the same detector. This is connected with the fact that the detector and the ionization chamber have different dead time constants and, therefore, if a drastic change in the intensity of the primary beam takes place, the ionization chamber contributes a considerably larger error as compared with a scintillator detector.

A collimation system is designed according to Kratki scheme and this allows one to receive the primary beam with low noise scattering. The slits are placed in a compact exhausted box. The size of a slit may be varied owing to the fact that the entire collimation system is rotated about the axis which is perpendicular to the SR beam. The collimation system is an automatic vertical stage identical to that installed at the monochromator.

A goniometer of the HGZ-4 type is placed in a radiation-safety hutch connected to the collimation system by a vacuum channel. The goniometer is adjustable for height using a vertical stage similar to that used when we adjust the monochromator.

The diffracted radiation is detected in the vertical plane. Such a detection scheme has been chosen because a) in this case, the beam plane after the monochromator is parallel to the goniometer axis and, hence, the whole beam aperture

may be used in the diffraction experiment and b) the SR beam polarization is used in an optimal way.

At the station, the detectors of two types are employed: an one-coordinate detector and a scintillator-detector. The first finds its application in experiments where there is no need in high angular resolution and only the information on the reflection intensity is required. The second-type detector is used in high-resolved diffraction experiment. For this purpose, Soller slits or a secondary monochromator is placed in front of the detector.

In what follows, a station for studying the solid-state chemical reactions by the 'in situ' Laue method using synchrotron radiation is described.

The X-ray method is referred to one of the basic ones dealing with solid-state chemical reactions and giving, in general, information on the position and elemental composition of atoms in the solid-state crystalline lattice. The X-ray diffraction method is a variety of the former and it gives information on the parameters of a lattice cell and on the position of the atoms of an object to be examined. In particular, the X-ray diffraction method in Laue geometry is an obtaining of X-ray diffraction pictures (Laue diffraction patterns) of a single crystalline object in the white X-ray beam. For a number of reasons (low efficiency of this way of X-ray exposure, impossibility to analyse and treat the relative intensity of reflections) this method is not often applied in defining the structure. As a rule, it is applied as an auxiliary means of research when analysing the symmetry of non-faceted crystals and especially when defining the crystal orientation. If the structure of the crystalline phase under investigation is however known, the dynamics of structural changes in the course of the chemical transformation can be established with an appropriate fast detection system available. DED-3M is a two-dimensional position sensitive multiwire X-ray detector and a device which can register in sequence several Laue diffraction patterns for a certain time interval and to store them digitized for their further computer processing. On the other hand, fast detection equipment can be efficiently used only in the conditions of fairly intense irradiation of the object to be studied. Synchrotron radiation (SR) can serve as the powerful source of radiation.

The problem of arranging the experiment 'in situ' is among the most complicated ones encountered in studies of solid-state chemical reactions. A particular substance is usually analysed prior to and/or after the reaction proceeds. In this case, during some time, when the sample under investigation is displaced from the reaction chamber at the place of analysis, the pressure and temperature are out of our control. This can give rise to some structural changes in the sample and to a substantially sophisticated interpretation of the experimental results obtained.

It follows from the above mentioned fact that X-ray studies of solid-state reactions should be performed in the time period during which a chemical reaction proceeds, i.e. the object being examined should be placed in the reaction chamber where the external conditions (atmosphere, pressure, temperature) necessary for the reaction to take place are satisfied; note that the chamber is in close vicinity to a detector and a radiation source.

The general layout of the station is as follows. The collimator forms a SR beam of 0.1-0.6 mm diam from the storage ring VEPP-3. The photon flux of the collimated beam at the sample site (single pole wiggler with H = 20 kG, E = 2 GeV, I = 100 mA) is 10^{11} photon/s. Arriving at and passing through the sample, the direct beam is catched by a trap and the diffracted radiation reaches the X-ray sensitive range of the DED-3M chamber. Thus, a direct (with respect to the passage) scheme of obtaining diffraction patterns in Laue geometry is realized. The sample is placed in the reaction chamber with given, by the reaction conditions, gaseous atmosphere (under definite pressure) or vacuum and temperature of the sample. To obtain a required initial Laue diffraction pattern there is a possibility of orienting the sample with respect to the incident SR beam in two mutually perpendicular axes of rotation Ω and φ . In the reaction chamber there are two beryllium windows for incident and diffracted radiation. The sample is a flat single-crystalline plate mounted in a crystal holder to provide heat contact. Instead of the reaction chamber the one-coordinate positioner with the crystal holder can be installed. The accuracy of the sample displacement relative to the SR beam is about 1 μm. The sample is moved perpendicularly to the incident beam direction.

The use of the station for the solid state reactions investigation was demonstrated during the study of the crystalhydrates dehydration as examples. These investigations can be performed in two ways. First, it is possible to study the kinetics of the structural change of the initial reagent during the dehydration. Second, taking into account the fact that the dehydration proceeds, as a rule, topochemically, it is also possible to study the reaction interface spatial structure.

The dehydration of the flat single-crystalline (z-cut) sample of $LiKC_4H_4O_6*H_2O$ was carried out in the vacuum P = = 0.1 Pa at 400 K. It may be concluded from these results that the reaction proceeds with the formation of the intermediate products.

Scanning (with a step of 50 μm) across the reaction interface by the SR beam (0.1 x 0.1 mm*mm) was performed on the partly dehydrated in vacuum single-crystalline (y-cut) sample of $CaSO_4*2H_2O$. The Laue diffraction patterns have been obtained during scanning of the reaction interface from the initial reagent to the dehydrated regions, $CaSO_4*5H_2O$ for this case. The lamination of the flaky gipsum structure in the interface is accounted for by band deformation distortion (the increase of the radial size of several reflections, for instance, $\bar{1}12$, $\bar{2}23$). Besides, there are relaxation processes of stored distortions in the reaction interface (the restruction of the $\bar{1}12$, $\bar{2}23$ reflections).

FIGURE CAPTIONS

Fig.1. Instrumental schem of the crystallographic station: 16 wiggler, 2- shutters, 3-slit sistem, 4-focusing monochromator, 5-trap, 6-slit, 7-focusing segmented mirror, 8-ionozation chamber, 9-Arndt-Wanacott sample holder, 10-photocamera.

Fig.2. Adjastment table with goniometer (view from above): 1-collimator, 2-carryng plate, 3- primary SR beam, 4-sample holder, 5-sample, 6-diffracted beam, 7-one-coordinate detector, 8-rotation stage, 9-vertical stage.

Fig.3. Changes in the wide-angle X-ray diffraction behaviour during heating of polyatilen.

Fig.4. Schematic experiment with microcollimation of an SR beam.

Fig.5. In the course of dehydration of $Li_2SO_4 \cdot H_2O$ some interplane distances, as well as d_{002}, are increased. The rest are not changed: (a) is a dash-diagram of the initial, interstitial and final structure, (b) is the dependence of the change of some interplane distances of a powder-like $Li_2SO_4 \cdot H_2O$ sample in the course of dehydration in vacuum.

Fig.6. Instrumental schem of the anomalous scattering station: 1-SR beam, 2-SR chanal, 3-slit, 4-rotation stage of monochromator, 5-double crystal-monochromator, 6-trap, 7-vertical stage, 8-slit, 9-beam-monitor, 10- Be foil, 11-goniometer, 12-sample, 13-secondary monochromator, 14- detector, 15-horizontal stage, 16-rotation stage.

Fig.7. Changes in X-ray diffraction pattern $YBa_2Cu_3O_{6,3}Br_x$ (x=1÷1,5)is caused by anomalous scattering effect. Designation above the patterns show the changes in the intensity at different energy (in %).

Fig.8. The general layout of the station for studing solid-state chemical reactions by Laue method.

Fig.9. Scanning of the $CaSO_4 \cdot 2H_2O$ reaction of dehydration interface by SR beam in the direction from the initial reagent to the final product. The scanning step is 50 μm.

Fig.10. Small angle diffraction pattern from the frog muscle, equatorial direction.

Fig.11. Time course of changes in small angle diffraction pattern in isometric contraction of frog muscle.

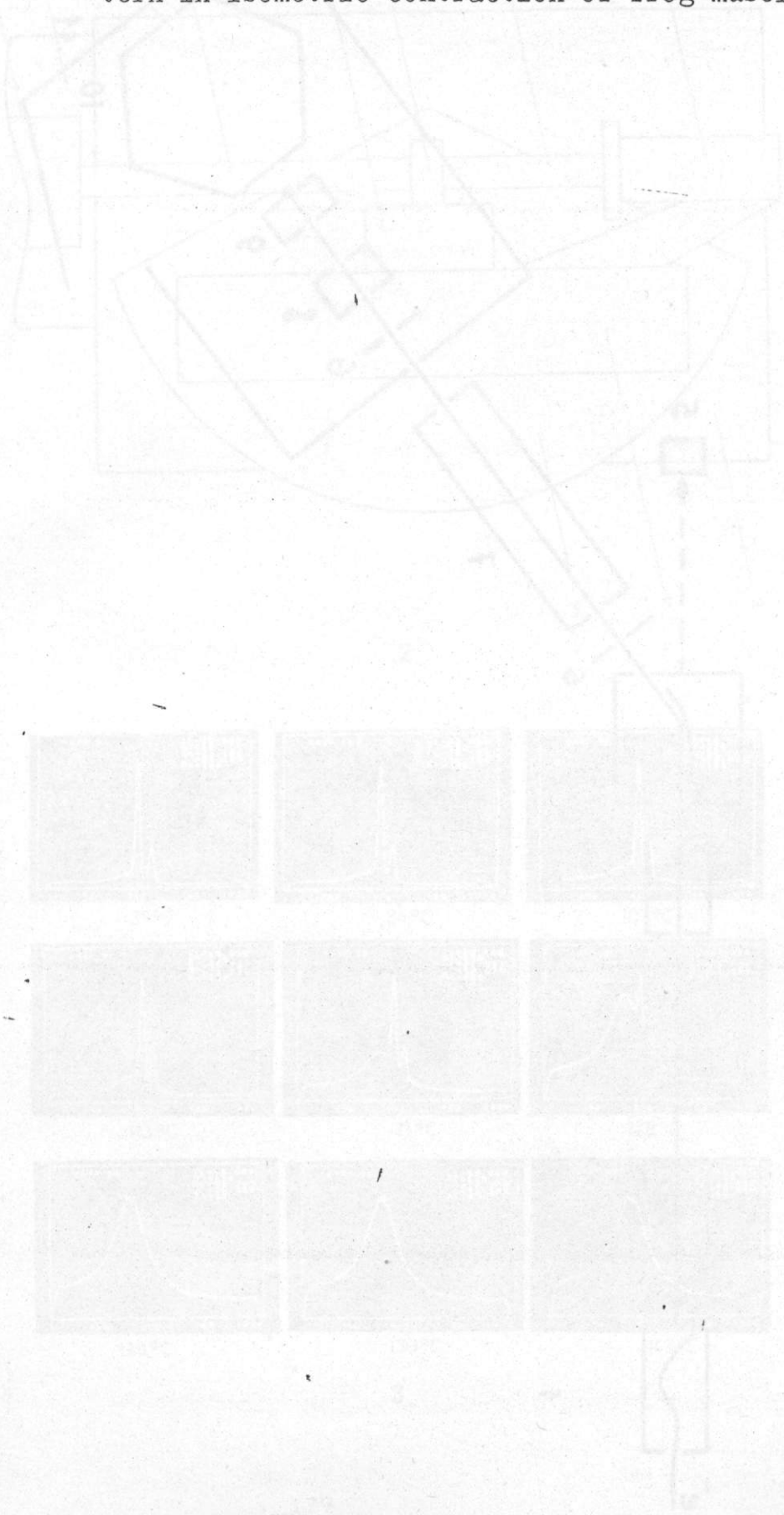

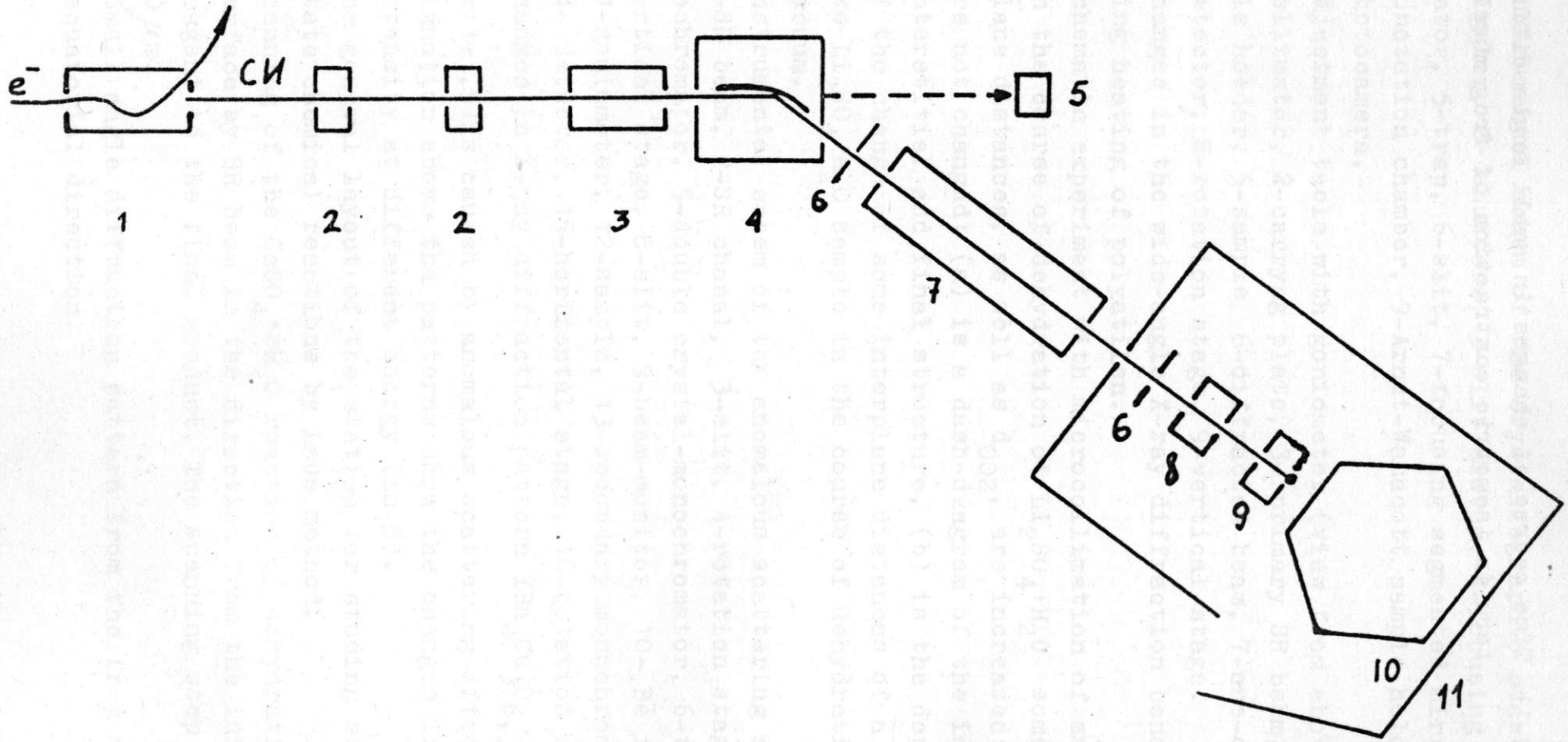
e⁻
CH
5
1
2
2
3
4
6
7
6
8
9
10
11

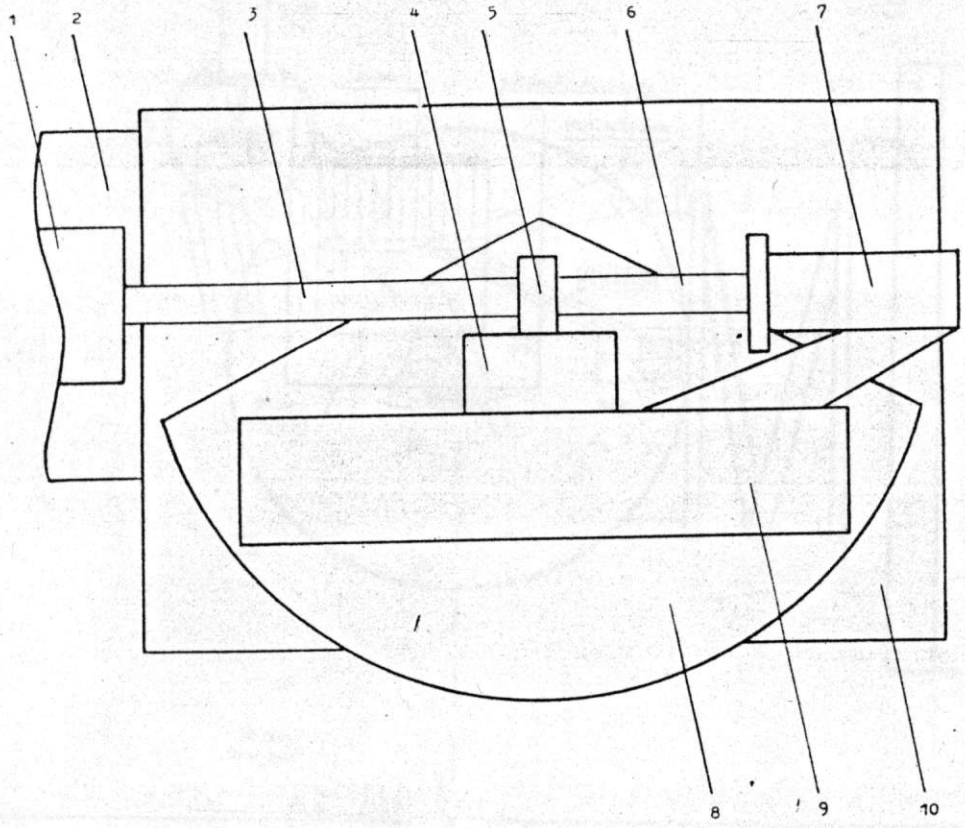

2.

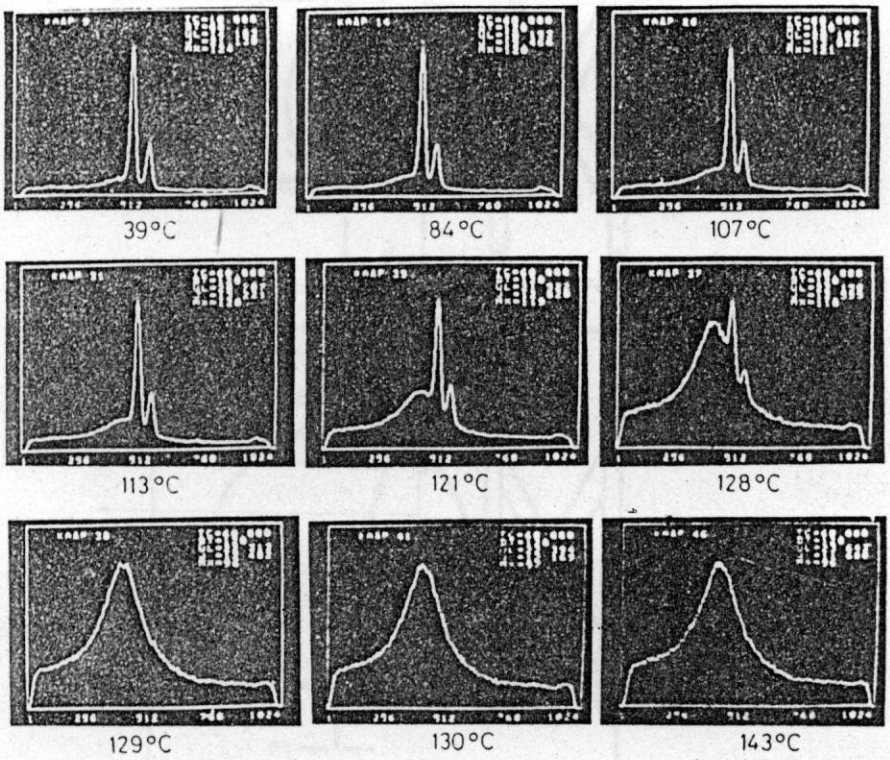

3.

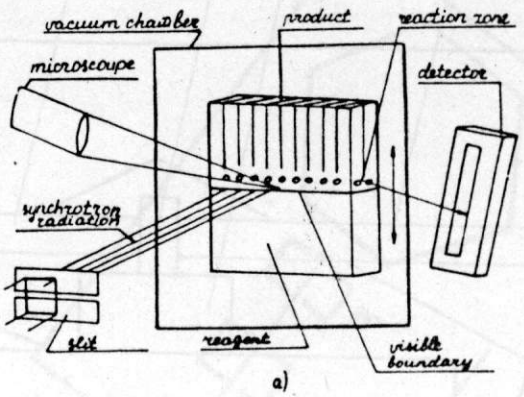
vacuum chamber
product
reaction zone
microscoupe
detector
synchrotron radiation
slit
reagent
visible boundary

a)

4.

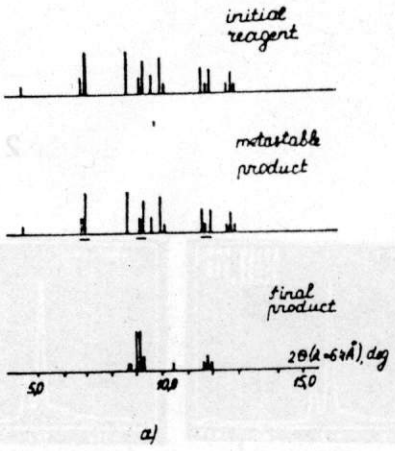
initial reagent
metastable product
final product
2θ(λ=6Å), deg
50
70
90

a)

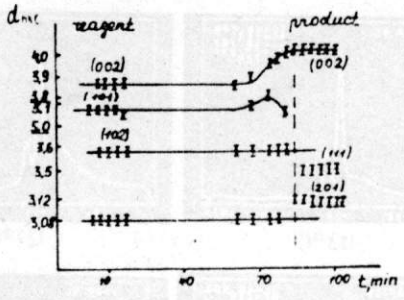
d, Å
reagent
product
4,0
3,9
3,8
3,7
3,6
3,5
3,4
3,3
(002)
(002)
t, min

в)

5.

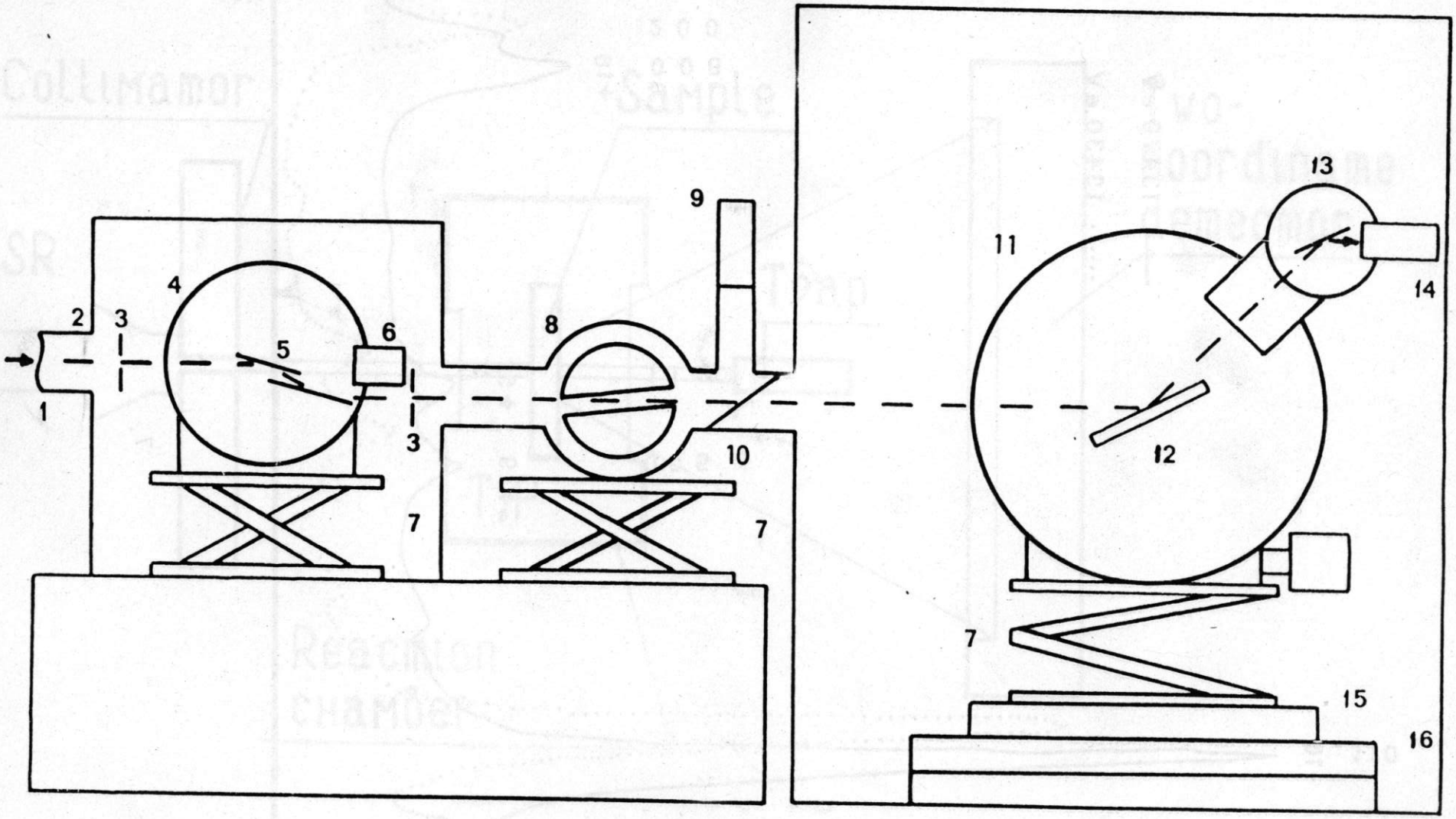

6.

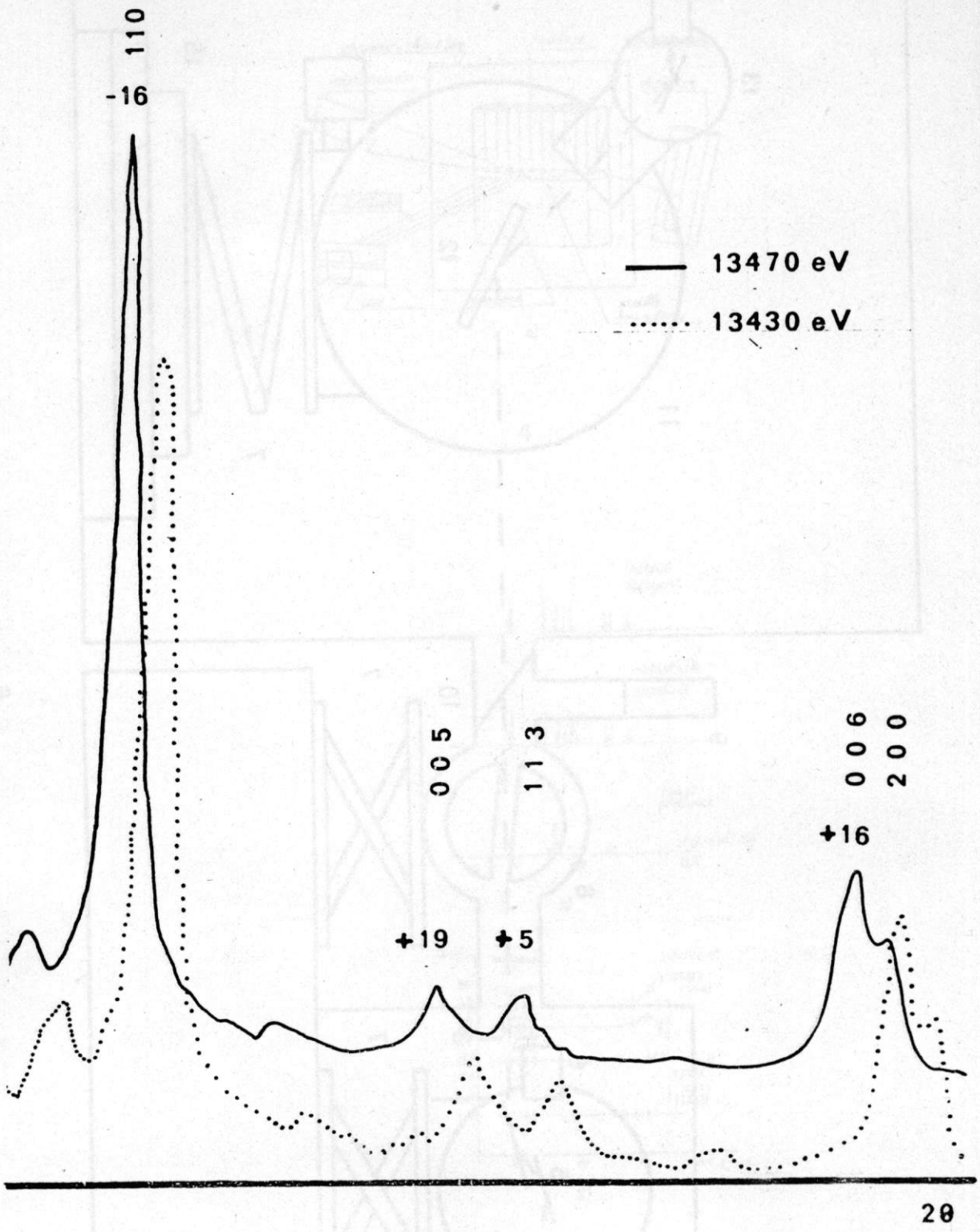

7.

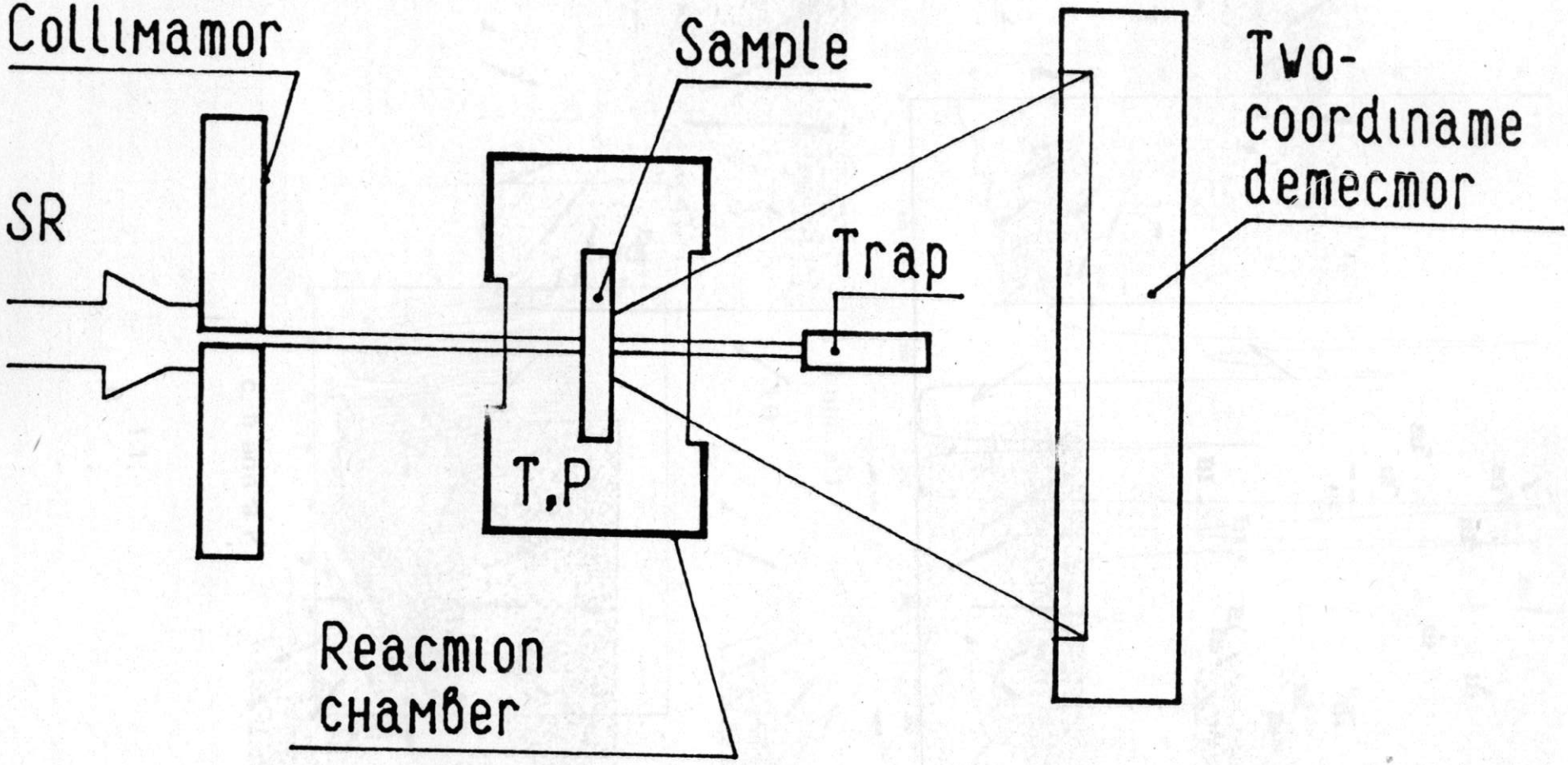
Collimamor
Sample
Two-
coordiname
demecmor
SR
Trap
T,P
Reacmion
chamber

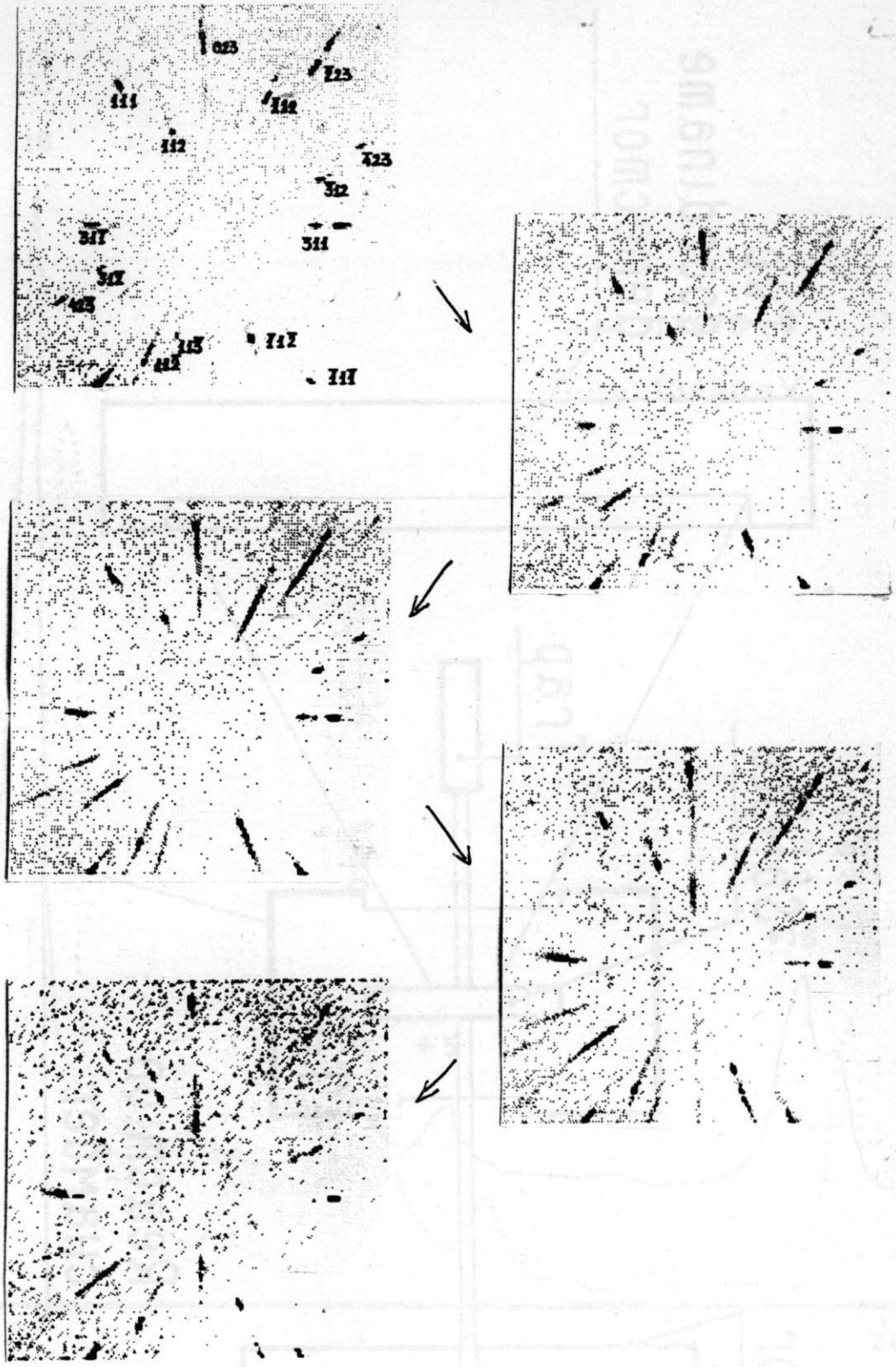

9.

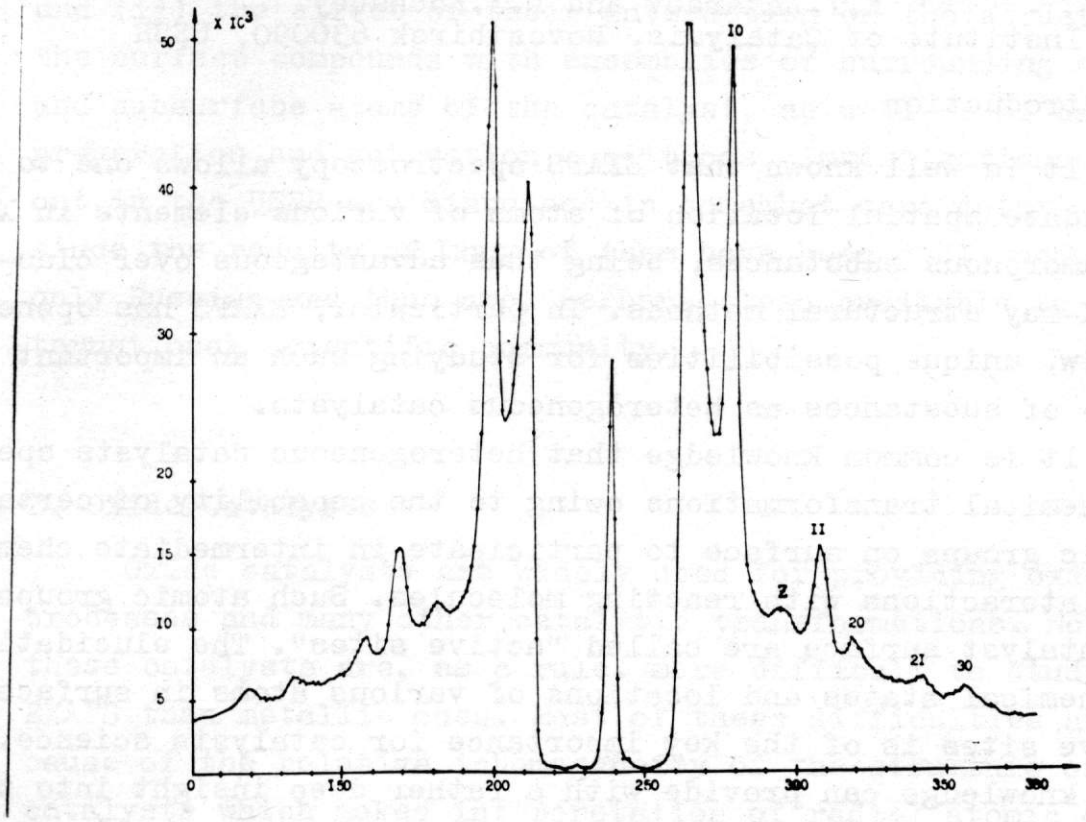

c h ann a l

10.

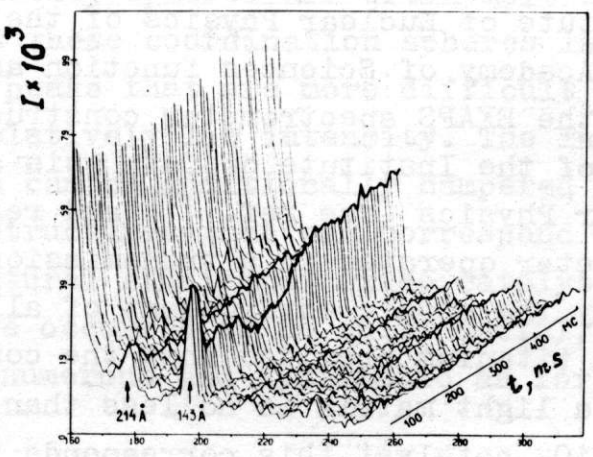

c h ann a l

11.